

The chemical composition of the cosmic radiation around the ankle and the related spectral indices

Antonio Codino ^a and François Plouin ^b

^aINFN and Dipartimento di Fisica dell'Università di Perugia, Italy.

^bFormer CNRS researcher , Ecole polytechnique, LLR, F-91128, Palaiseau, France.

Some recent measurements of the chemical composition of the cosmic radiation indicate that at the energy of 3×10^{18} eV, around the ankle, light cosmic ions dominate the spectrum as it occurs in the pre-knee energy region. Taking advantage of a recent theory of cosmic radiation which provides a quantitative explanation of the knee, the second knee and the ankle, the chemical composition of cosmic radiation is explicitly calculated giving individual ion spectra and ion fractions from 10^{12} eV to 5×10^{19} eV. The calculation assumes two components of the cosmic radiation feeding the ion flux at Earth: one originated in the disc volume and another one, called *extradisc component*, which from the disc boundaries traverses the Galaxy reaching the solar system. Data above 10^{17} collected during half century of experimentation by Auger, HiRes, Agasa, Akeno, Fly' s Eye, Yakutsk, Haverah Park and Volcano Ranch experiments are reviewed, examined and compared with the theoretical $\langle \ln(A) \rangle$. The comparison between computed and measured $\langle \ln(A) \rangle$ exhibits a good global accord up to 2×10^{19} eV except with the HiRes experiment and an excellent agreement in the range 10^{15} - 10^{17} eV with Kascade, Eas-top, Tunka and other experiments. The accord requires a flux of the extradisc component of 1.8×10^{14} particles/(m^2 sr s $eV^{1.5}$) at 10^{19} eV, twice that generated by disc sources.

1. Introduction

The spectrum ¹ of the cosmic radiation between the knee and the ankle has been recently calculated according to the *Theory of Constant Spectral Indices* [1-4]. The galactic mechanisms and the parameters generating the knee are the same at the origin of the ankle: this circumstance constitutes a major characteristic of the solution of the knee and ankle problem. Another notable aspect of this solution is the presence of a structure at $(5 - 7) \times 10^{17}$ eV which is called the second knee, just a direct consequence of the theory [5]. Figure 1 shows an example of excellent quantitative accord between computed and measured cosmic-ray spectrum [4].

The *Theory of Constant Spectral Indices* determines the energy spectra of individual ions, or group of ions, in the interval 10^{11} - 5×10^{19} eV with only one normalization point for the par-

ticle flux. As a consequence, once the spectral indices and the abundances at a given energy are assigned, the chemical composition of the cosmic radiation is known at any energy. Fig. 2 shows that individual ion spectra in the knee energy region are also in good agreement with the theory. The simplicity of the theory and its anchorage to the empirical parameters governing the cosmic-ion motion in the Galaxy are not minor aspects besides the excellent quantitative agreement with ion spectra exhibited in figures 1 and 2.

The chemical composition expressed by $\langle \ln(A) \rangle$ has been also calculated with all cosmic-ray sources placed in the disc [6], thus ignoring any extragalactic component. Figure 3 reports the results of the calculation. The profiles of $\langle \ln(A) \rangle$ measured by the Kascade and Tunka experiments along with that extracted with the measurements of X_{max} of the Auger Collaboration are shown in figure 3. There is an evident disagreement above 10^{17} eV between theory and data. All other experiments above 10^{17} eV have been purposely omitted from figure 3 to render

¹ This paper is an english translation of an INFN Report to be published in italian: *Composizione Chimica della Radiazione Cosmica intorno alla Cavaglia e Indici Spettrali*

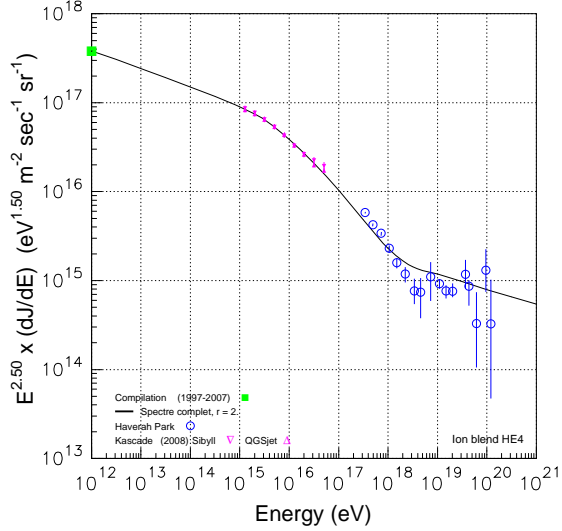


Figure 1. The differential cosmic-ray spectrum (black thick line) resulting from the theory normalized to 3.79×10^{17} particles/(m^2 sr s $eV^{1.5}$) at 10^{12} eV (green square). The data are from the Cascade [7] and Haverah Park [8] experiments.

the disagreement between theory and data more evident. According to the above quoted measurements the theoretical chemical composition, as generated by the galactic cosmic-ray sources above 4×10^{17} eV, is incompatible with the data, primarily because it is too heavy, and secondly, because above 2×10^{19} it has a flat trend, contrary to the measured $\langle \ln(A) \rangle$, which increases with energy.

Notice that the Auger Collaboration disposes today (2009) of a powerful and redundant apparatus and a number of recorded atmospheric cascades superior to that of any other experiment.

The purpose of this work is to calculate the chemical composition of the cosmic radiation at Earth, not only assuming cosmic-ray sources in the disc, but also postulating a component that penetrates the disc volume from the exterior reaching the Earth. This cosmic-ray component is called here *extradisc* being a particular component of the more vast class of the extragalactic cosmic rays.

Both the extradisc cosmic rays and their flux will be denoted by the same symbol I_{ed} (*ed* for

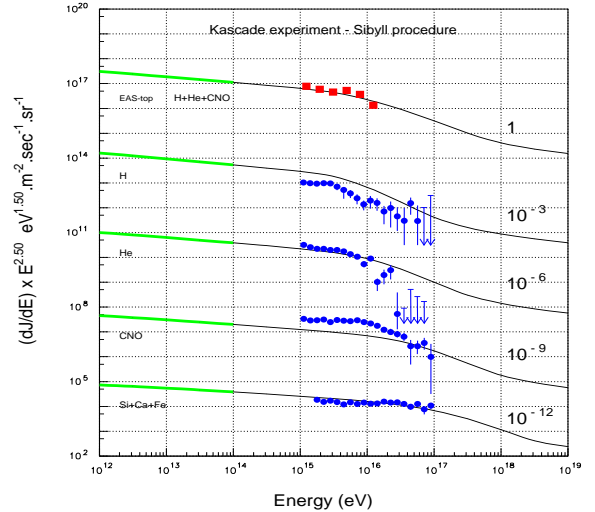


Figure 2. Energy spectra of individual ions and group of ions of Eas-top (red squares) [9] and Cascade (blue small circles) [10] experiments compared with the theory of constant spectral indices (black curve). Fluxes are normalized at 10^{12} eV. Ion grouping and flux of the Eas-top experiment shown in this figure are examined elsewhere [11].

extradisc). Let us anticipate here that *extradisc component* reconciles the results of the theory with the Auger data on $\langle \ln(A) \rangle$ shown in figure 3, still preserving a quantitative accord with the knees, the ankles and the second knee.

The structure of this paper preassumes the existence of the *Theory of Constant Spectral Indices* [1-4] and the companion paper [6] where the chemical composition of the cosmic radiation is evaluated under the restricted assumption that all cosmic-ray sources feeding the particle flux at Earth are placed in the disc volume. Section 2 presents a brief survey of the bases of the calculation and a flash of the cultural background of the theory. Section 3 is devoted to a survey on cosmic-ion energy spectra useful for the normalization of the theory at 10^{12} eV. Section 4 summarizes the calculation of the chemical composition obtained with the galactic sources only. Section 5 reports a comparison between data and theory under the assumption that all cosmic ray sources

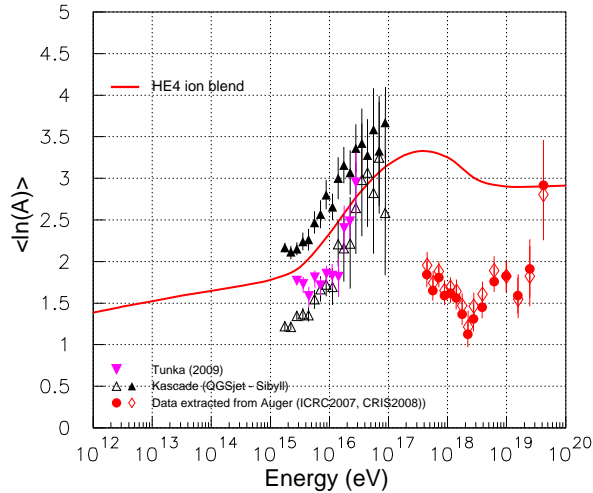


Figure 3. Comparison of the $\langle \ln(A) \rangle$ derived from the *Theory of Constant Indices* with the Tunka [13], Kascade [14] and Auger [15] data. A significant discrepancy between this calculation and the Auger data appears above 4×10^{17} eV. The theoretical evaluation of $\langle \ln(A) \rangle$ (blue line) assumes that all cosmic-ray sources are placed in the disc volume, with no extragalactic component.

are placed in the disc and not in its exterior. Section 6 reports many details of the calculation of the ion abundances of the *extradisc component* and the attenuation of its intensity while penetrating the disc volume from its periphery up to the solar system.

The results of the calculation reported in Section 6 are utilized in Section 7, where the $\langle \ln(A) \rangle$ for the disc and extradisc components are given. The comparison of the predicted $\langle \ln(A) \rangle$ with the data for the two components I_{ed} and I_d (disc component) are given in Sections 8 and 9. Section 10 marks the disagreement on the chemical composition between the HiRes experiment and others. Conclusions are in the last

Table 1

Parameters of the theory denoted Low Energy (*LE*) and High Energy (*HE*) ion blends. Fluxes are multiplied by $E^{2.5}$ and expressed in units of ($m^{-2}sr^{-1}s^{-1}eV^{1.5}$).

Blend.	LE		HE	
	10^{12} eV		10^{14} eV	
	%	γ	%	γ
H	42.4	2.77	33.5	2.67
He	26.5	2.64	27.3	2.64
CNO	11.9	2.68	13.6	2.65
Ne-S	9.2	2.67	10.9	2.63
Ca(17-20)	1.2	2.67	2.8	2.63
Fe(21-28)	8.7	2.59	12.0	2.62
	Flux	γ	Flux	γ
H	$1.15 \cdot 10^{17}$	2.77	$3.93 \cdot 10^{16}$	2.67
He	$7.19 \cdot 10^{16}$	2.64	$3.20 \cdot 10^{16}$	2.64
CNO	$3.24 \cdot 10^{16}$	2.68	$1.60 \cdot 10^{16}$	2.65
Ne-S	$2.50 \cdot 10^{16}$	2.67	$1.28 \cdot 10^{16}$	2.63
Ca(17-20)	$3.14 \cdot 10^{15}$	2.67	$3.27 \cdot 10^{15}$	2.63
Fe(21-28)	$2.36 \cdot 10^{16}$	2.59	$1.41 \cdot 10^{16}$	2.62
Total	$2.71 \cdot 10^{17}$	2.70	$1.18 \cdot 10^{17}$	2.64

Section 11.

2. Bases and foundation of the calculation

A prerequisite inherent this calculation states that cosmic rays generated in the disc volume of the Milky Way might migrate into the halo, and eventually, into the intergalactic space [6]. The disc of Milky Way is regarded as standard, typical disc volume. All these cosmic rays escaped from the disc volume populating the extradisc space, constitute the *extradisc component*. This calculation admits that a fraction of the extradisc component existing at the outskirts of the disc volume, by displacement predominantly shaped by the the magnetic field and gas density, can reach the solar cavity (the Earth): its intensity will denoted by I_{ed} .

In order to perform practical calculation it is necessary to specify some properties and features of the extradisc cosmic rays present outside the disc:

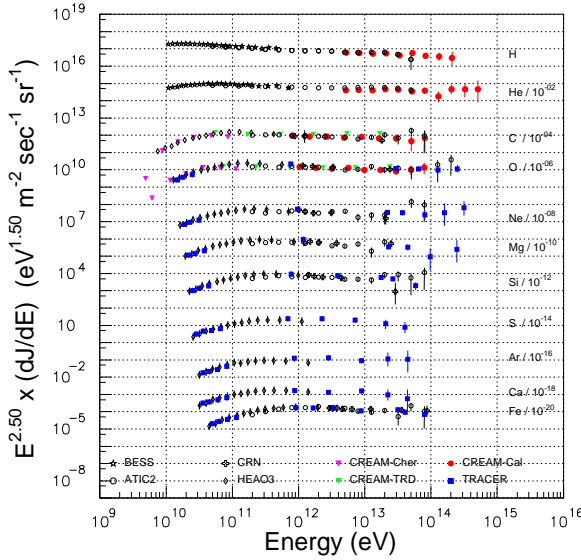


Figure 4. Energy spectra of 11 individual ions measured by balloon and satellite detectors at energies below 10^{15} eV suggesting and founding the postulate of the constant spectral indices (see ref. [16] and references therein).

(A) Cosmic rays emitted by the sources placed in the disc and escaping from the disc volume undergo alterations of their abundances as released at the sources, due to nuclear interactions with interstellar gas. It will be shown that this alteration depend both on the energy and the type of the ion.

(B) The spectral index of any ion released at the sources in the disc volume is constant in the energy interval 10^{11} - 5×10^{19} eV. The plausibility of this fundamental hypothesis is rooted on the measurements of the spectral indices collected in more than half a century by balloon and satellite detectors (see fig. 4, 5 and 6). This hypothesis

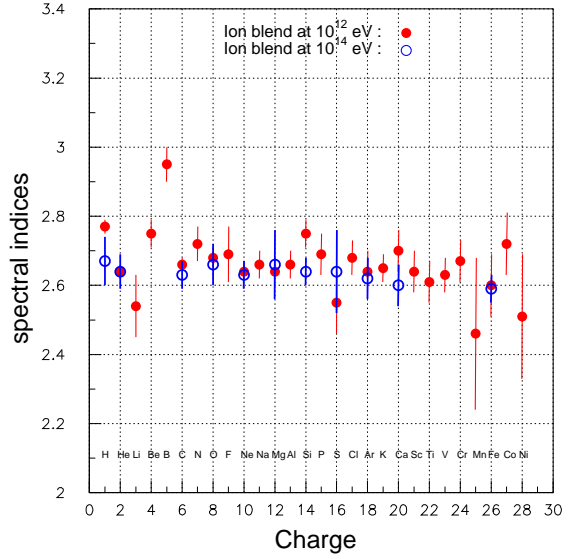


Figure 5. Spectral indices of cosmic ions from Hydrogen to Nickel measured by balloon-borne and satellite detectors at 10^{12} eV (filled red dots) and 10^{14} eV (open blue dots). All indices extracted from the spectra around 10^{14} eV fall between 2.6 and 2.7.

has been converted in 2006 into a postulate called *Postulate of Constant Spectral Indices* [1].

(C) Ion abundances as a function of energy of the extradisc particles traversing the disc and arriving at Earth are evaluated assuming the same parameters adopted for the disc component I_d .

Though the present calculation ignores the mechanism that accelerate cosmic rays in the Milky Way, two constraints have to be obeyed by the accelerator, whatever it might be, in the range 10^{11} - 5×10^{19} eV : (1) spectral indices generated at the sources placed in the disc volume are independent of energy; (2) the cosmic-ray sources are uniformly distributed in the disc volume at any energy [12].

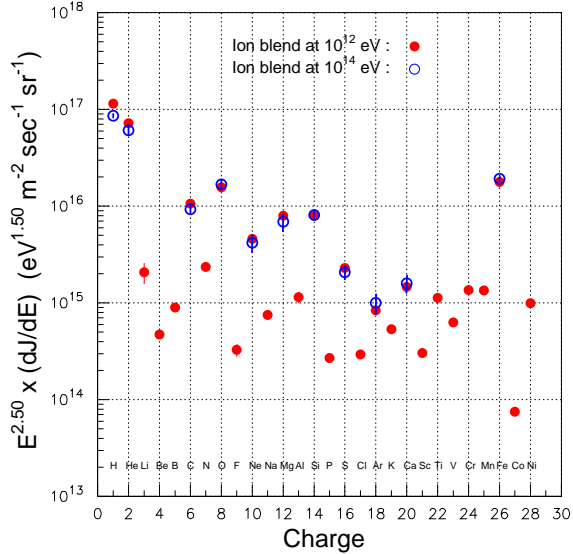


Figure 6. Measured fluxes of individual ions of the Wiebel-Sooth Compilation (*LE* blend) (red dots) and *HE4* Compilation (open blue dots).

It has been demonstrated by full simulation of cosmic-ray motion that the displacement of the cosmic rays from the sources to any point in the Galaxy has a modest effect on the spectral indices released at the sources. For example, the propagation of helium in the disc entails an index modification of 0.04 in the energy band 10^{12} - 10^{14} eV being at the sources 2.65. While for most calculations this index modification is a negligible effect, for the evaluation of the chemical composition around the ankle is of quite notable importance.

The interval of application of the *Theory of Constant Spectral Indices* is 10^{11} - 5×10^{19} eV. The upper energy extreme is determined by the realization that the characteristics of the knee and the ankle of the *complete spectrum* (all-particle spectrum) are quantitatively explained by the theory. The theory predicts the exact position where the ankle is observed, at $(4-5) \times 10^{18}$ eV and that of the knee as well, and many other features. The quantitative characteristics of the ankle of the *complete spectrum* derive from those of the ankles of the individual ions. The proton ankle is at the lowest energy while the iron ankle is at the maximum energy, which turns out to be 5×10^{19}

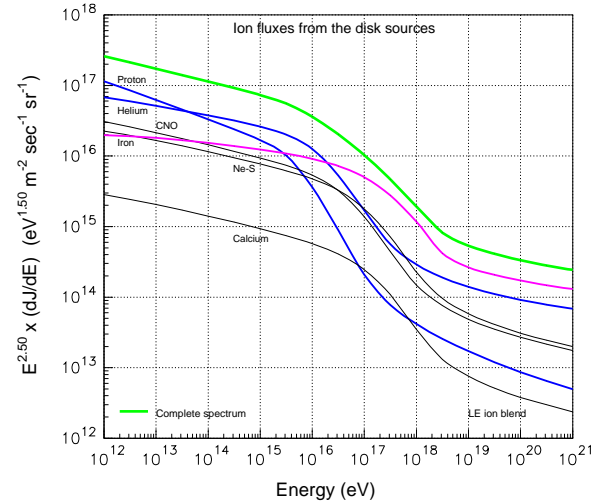


Figure 7. Theoretical spectra of 6 ions for the *LE* blend and the resulting *complete spectrum* (thick green upper curve).

eV.

The theory distinguishes an ankle in the grammage versus energy and an ankle in the cosmic-ray intensity versus energy. The knees are intimately related by the theory to the ankles of any ions, and since there exist an excellent quantitative agreement with numerous experimental data, the maximum energy involved in the knee-ankle relationship is the Fe ankle energy. The Fe ankle energy in the grammage is at 5×10^{19} eV, and as a consequence, it delimits the range of application of this theory. Above the energy of 5×10^{19} eV the results reported in this paper and the companion one [6] have to be regarded as numerical exercises. In fact, physical phenomena having empirical evidence operate above 5×10^{19} eV but they are not incorporated in the *Theory of Constant Spectral Indices* as it is presently formulated [1,2,3,4].

The results of the calculations depend on the geographic site of the sources generating the extradisc component. For instance, if the sources of the extradisc component would be the ensemble of the spiral galaxies, due to the similarity of the Milky Way Galaxy, only minor modifications of the calculations would be necessary to deter-

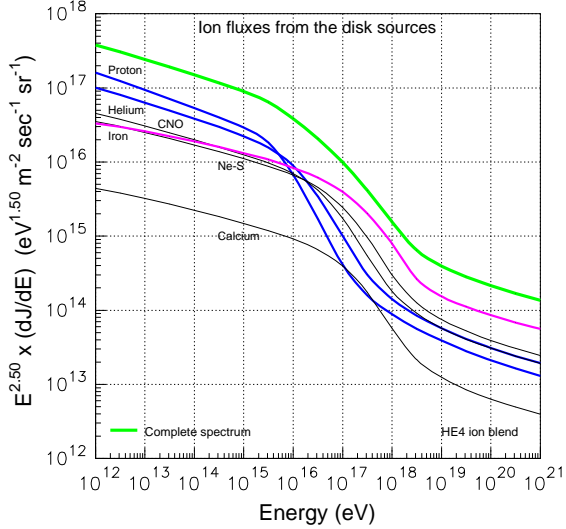


Figure 8. Theoretical spectra of 6 ions for the HE4 ion blend and the resulting *complete spectrum* (thick upper green curve) normalized at 10^{12} eV with a flux of 3.89×10^{17} particles/ m^2 sr s $eV^{1.5}$.

mine $\langle \ln(A) \rangle$. If the sources of the extradisc cosmic rays would be placed in the local Supercluster of galaxies, the present calculations are not sufficiently precise for a number of reasons. If the extradisc component are just reentrant particles escaped from the disc of the Milky Way, as already suggested [2], the calculations are exact.

Total kinetic energy of particles is used everywhere in this paper.

3. Measurements of the spectral indices and ion abundances

Let us preliminarily notice that the interpolation of the energy spectra of individual ions with a constant spectral index in a restricted energy band it is an established tradition at energies below 10^{15} eV. An index slightly depending on energy would probably conform better to some data, in some energy intervals. This refinement, however, it is still uncommon, and unnecessary in the present work, and consequently omitted here.

The fundamental hypothesis of the present calculation incorporated in the *Theory of Constant Spectral Indices* is that all ions at the sources have

Table 2

Parameters of the theory at 10^{12} eV denoted universal and HE4 ion blends. Fluxes are multiplied by $E^{2.5}$ and expressed in units of ($m^{-2}sr^{-1}s^{-1}eV^{1.5}$).

	HE4		Universal	
	%	γ	%	γ
H	42.4	2.74	37.2	2.645
He	26.5	2.72	26.4	2.640
CNO	11.9	2.69	13.9	2.650
Ne-S	9.2	2.68	10.1	2.650
Ca(17-20)	1.2	2.67	01.5	2.650
Fe(21-28)	8.7	2.66	10.8	2.650
	Flux		Flux	
H	1.61E+17		8.60E+16	
He	1.01E+16		6.10E+16	
CNO	4.54E+16		3.22E+16	
Ne-S	3.50E+16		2.34E+16	
Ca(17-20)	0.44E+16		0.34E+16	
Fe(21-28)	3.31E+16		2.50E+16	
Total	3.89E+17		2.31E+17	

constant spectral indices.

This simple hypothesis predominantly concurs in the prediction of the *complete spectrum* leading to the excellent agreement with experimental data as shown, for example, in figure 1.

Figure 4 reports the energy spectra of 11 different ions in the interval 10^{10} - 10^{15} eV. The spectra form a grid of parallel straight lines in the flux units shown. *A posteriori* the regular forms of these spectra with no dips and no spikes justify the postulate of *Constant Spectral Indices*. Though the evidence for constant indices is solid and irrefutable below 5×10^{16} eV there exist in *Nature* magnificent and universal phenomena that modify indices released at the sources. The ensemble of the processes referred to as solar modulation occurring in all stars is an example of violation of the *Postulate of Constant Spectral Indices* at low energy. Thus, local phenomena evidently violates the postulate. In order to ascertain if additional local phenomena in the Galaxy, besides solar modulation and the knees, in the interval 10^{11} - 5×10^{19} eV alter the indices, a careful

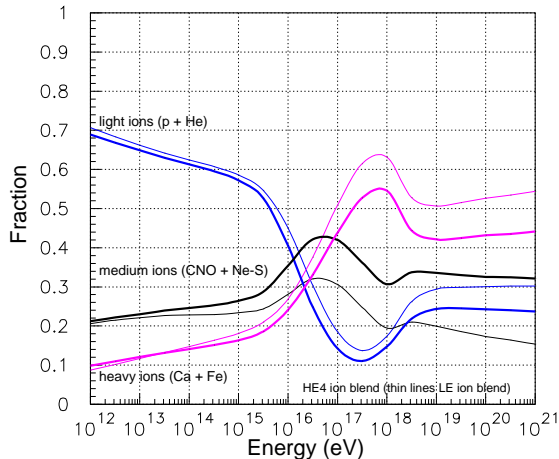


Figure 9. Relative amounts of light, intermediate and heavy ions versus energy for the LE (thin curves) and HE (thick curves) ion blends. Notice the minimum of the light component around 3×10^{17} eV in both ion blends, followed by a stable increase of the light ion fraction up to 4×10^{18} eV.

examination of the experimental data is mandatory.

A compilation of indices of a number of nuclides from Hydrogen to Nickel is shown in figure 5. This compilation based on measurements of the indices mainly between 10^{10} - 10^{15} eV is referred to as Wiebel-Sooth compilation [17] and the corresponding parameters incorporated in the theory are called *LE ion blend* (Low Energy). Another compilation of spectral indices collecting measurements at higher energies [16] between 10^{12} - 10^{15} eV is also shown in the same figure 5 (blue open dots) and it is referred to as *HE ion blend* (High Energy). The spectral indices shown in figure 5 accumulate around a common value of 2.65 between 10^{11} - 10^{15} eV. It is also evident from the experimental data on the indices shown in figure 5 (red dots) that higher the atomic mass harder the index. This correlation between indices and atomic mass is more pronounced for *LE* than *HE4* ion blend.

Notice that the parameters of the Wiebel-Sooth Compilation incorporated in the *LE* ion blend based on the interval $10 \times Z(\text{GeV})$ up to 10^{12} eV

are three orders of magnitudes from the knee energy region (e.g. 10^{15} - 10^{18} eV) while those of the *HE* ion blend are closer. If the postulate of the constant spectral indices is exactly described by a straight line (in logarithmic scales of intensity and energy) either the *LE* or *HE* blend would suffice to correctly calculate the chemical composition. In this circumstance the differences in the chemical composition at any energy are only due to the ion abundances at the normalization energy of the theory. If quite small violations of the postulate take place, then, the differences originating from the two ion blends become significant.

Recent experimental data between 40 and 400 *GeV* indicates that the proton index changes from 2.77 ± 0.02 to 2.67 ± 0.03 in the interval 4×10^{14} to 4×10^{15} eV taking into account the data of Atic2 [18] and Cream experiments [19].

The hardening of the index seems to affect the helium spectrum as well. In fact, the index of 2.70 ± 0.02 measured at low energy below 400 *GeV* decreases to the value of 2.62 ± 0.05 above 400 *GeV* up to the maximum energy explored to day of 4×10^{14} eV [20]. The alteration of the H and He indices in the pre-knee energy region would entail a change in the H/He flux ratio which has been proved to be constant at low energy, 10^{13} eV [21]. The H/He flux ratio versus energy has been examined in another paper [16] where it has been shown that the problem of the H/He flux ratio above 10^{13} eV, is, at the present times, inextricable. The recent data of the Cream experiment [22] do not resolve the problem of the H/He flux ratio below 10^{15} eV due to the large error bars of the experiment at high energy, in the decade 10^{14} - 10^{15} eV.

Figure 6 reports the ion fluxes for the 2 compilations defining the parameters of the *LE* and *HE* blends. The fluxes are almost equal for the two blends as shown in fig. 6. The flux of the complete spectrum based on the Wiebel-Sooth compilation (*LE* blend) is 2.71×10^{17} particles/ m^2 s sr $eV^{1.5}$ at 10^{12} eV. The *HE* blend at 10^{12} is normalized at the same flux which at 10^{14} eV becomes 1.07×10^{17} particles/ m^2 s sr $eV^{1.5}$. The complete spectrum has been measured in the region 10^{12} - 10^{15} giving a spectral index of 2.74 and an extrapolated intensity at 10^{12}

around 2×10^{17} particles/ m^2 s sr $eV^{1.5}$ [23].

In the interval 10^{15} - 10^{17} eV recent flux measurements of the complete spectrum by Cascade give (Sibyll) 7.68×10^{16} and (QGSjet) 7.48×10^{16} particles/ m^2 s sr $eV^{1.5}$ at the reference (and arbitrary) energy of 2×10^{15} eV. Statistical errors of these measurements are about 7 per cent. Note that the difference in the *complete spectra* resulting from QGSjet and Sibyll algorithms is negligible (see fig. 1). Differences in flux measurements resulting from QGSjet and Sibyll algorithms become quite significant for individual ions amounting to factors 2-10 for some ions in some energy intervals as pointed out elsewhere (see Section 9 of ref. [11]).

The Cascade data suggest that the spectral indices of heavy ions are constant in any pre-knee energy region. Empirically, they are expected to be constant on the basis of balloon and satellite data on proton and helium spectra collected below 10^{15} eV, provided that the H and He knees are regarded as experimentally observed, around 2×10^{15} eV and 6.7×10^{15} eV, respectively. If so, heavy ion spectra are expected to behave similarly.

The heavy ion spectra measured by the Cascade experiment do have constant spectral indices close to 2.65 [24,25]. Any methods of analysis (QGSjet, Sibyll or deconvolution method) yield indices of about 2.65² or harder but not softer. When harder indices are observed a contamination between nearby ions is suspected or demonstrated (see Section 7 of ref. [11] devoted to this argument). With the appropriate ion groupings of contaminated adjacent ion samples and the correct guide from the theory [1-4], a constant common index for heavy ion spectra in the fundamental energy region 10^{15} - 10^{17} emerges [11].

Though the present calculation does not depend on any acceleration mechanism, a theory

² In the paper : *The Transition from Tortuous to Rectilinear Cosmic Ray Trajectories is at the Origin of the Knee* by A. Codino and F. Plouin [4], the theoretical Fe spectrum is compared with that measured by the Cascade experiment, which has an index of 2.64 ± 0.06 . In this comparison heavy ions include nuclei from Silicon to Nickel. Different groupings result in similar indices but always in overabundant fluxes compared to the theory (see figs. 16 and 17 of ref. [5]).

of cosmic-ion acceleration in pulsar atmospheres having constant spectral indices up to 5×10^{19} eV has been conceived in 1969 [26].

The findings on the indices of heavy ion spectra of the Cascade experiment consolidate the *Postulate of Constant Spectral Indices* from 10^{15} eV up to about 10^{17} eV (unobserved Fe knee). As far as the *Postulate of Constant Indices* is at stake, the outcomes of the Cascade experiment on heavy ion spectra in the interval 10^{15} - 10^{17} eV have anticipated, probably by more than half a century, those plausibly expected by future balloon and satellite experiments, which identify individual ions with superior discrimination power but with a very few nuclei.

The data shown in figure 5 are included in the theory with 6 indices and 6 fluxes at the normalization energy of 10^{12} eV. The values of these parameters are given in Table 1.

In the same Table 1 are given the parameters of the *HE* blend tuned to the data at higher energy. In the following, in order to appreciate differences and similarities with previous calculations, the parameters of 2 additional ion blends referred to as universal and *HE4* blends are given in Table 2. In the universal ion blend all indices are equal with a value of 2.65 except for helium set at 2.64 which takes into account the recent trend of the measurements suggesting an index harder than that of other ions. The *HE4* blend is a variant of the *HE* blend where the dominant nuclei, e.g. protons and helium, H and He have the classical value of 2.74 [23] and 2.72 [27] believed for many years to be standard, reliable measurements. The parameters of the *HE4* blend are used to determine the chemical composition around the ankle (see fig. 6). The *HE4* blend is normalized at 10^{12} eV with a flux of 3.79×10^{17} particles/ m^2 s sr $eV^{1.5}$. This value is inspired from the Cascade flux measurement which is 7.58×10^{17} particles/ m^2 s sr $eV^{1.5}$ at 2×10^{15} eV (mean value of QGSjet and Sibyll algorithms) [7]. The *HE4* flux normalization at 10^{12} eV is larger than that of the *LE* blend (Wiebel-Sooth flux compilation) by a factor 1.4.

Because of the ion propagation in the disc volume the indices of the original spectra released by the sources modify (see fig. 6 of ref. 3).

It may be useful to subdivide the index of any ion spectrum measured at the solar cavity in two parts: the propagation index and the accelerator index at the sources. The propagation indices due to ion displacement in the disc volume for the 6 ions H, He, N, Si, Ca and Fe are, respectively, 0.060, 0.055, 0.045, 0.045, 0.040 and 0.040. Taking into account the accelerator indices of the universal blend (see Table 2) the global index become: 2.585, 2.585, 2.605, 2.605, 2.610 and 2.610 for the same ion sequence just mentioned.

4. Chemical composition of the cosmic radiation generated by cosmic-ray sources placed in the disc

The energy spectra of 6 ions derived from the *Theory of Constant Spectral Indices* with the *LE* and *HE4* blends are, respectively, in figure 7 and 8. The *complete spectrum* which is the sum of the *partial spectra* of individual ions is also shown in the same figures 7 and 8 for both blends resulting in a flux of 8.2×10^{16} particles/ m^2 s sr eV^{1.5} for the *HE4* ion blend at 10^{15} eV. The ion abundances derived from the energy spectra reported in figures 7 and 8 are shown in figure 9 for the interval 10^{12} - 5×10^{19} eV. The light ion fraction (H+He) decreases with a gentle slope going from 68 per cent at 10^{12} eV to 55 per cent at 1.5×10^{15} eV (*HE4* ion blend). Above this energy the light ion fraction descends abruptly reaching a minimum of 11 per cent at the energy of 4×10^{17} eV, quite evident in figure 9. A similar behaviour is exhibited by the *LE* blend but with higher light ion fractions.

The slight increase in the (Ca+Fe) fraction in the interval 10^{12} - 4×10^{15} eV for the *HE4* blend is caused by the tiny difference in the Ca and Fe slopes (2.66 for Fe and 2.650 for Ca, see Table 2) with respect to the light ion slopes (2.74 for H and 2.72 for He). The strong increase of the (Ca+Fe) fraction between 4×10^{15} eV and 7×10^{17} eV is due not only to the difference in the indices (2.70 light ions against 2.60 heavy ions) but predominantly to the high fall of the light ion flux (light ion knees) above the nominal knee of the complete spectrum at 3×10^{15} eV. The fall is quite notable for protons and helium in the inter-

val 2×10^{15} - 2×10^{17} eV but insignificant for heavy ions (Ca+Fe) at least up to 4×10^{17} eV. The processes causing this abrupt fall of intensity (knees) have been analyzed and described elsewhere [3].

5. The $\langle \ln(A) \rangle$ of cosmic-ray disc component compared with the data

It is instructive to compare the theory with the experimental data on $\langle \ln(A) \rangle$ under the restricted assumption that all cosmic-ray sources are in the disc volume with no extragalactic component.

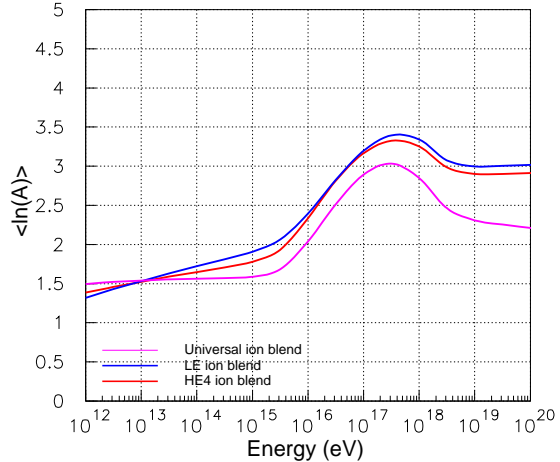


Figure 10. Mean logarithmic mass of the cosmic radiation resulting from the *Theory of Constant Indices* in the energy interval 10^{11} - 5×10^{19} eV for three ion blends. In these 3 evaluations all cosmic-ray sources are placed in the disc volume.

The ion spectra shown in figure 7 or 8 directly determine the chemical composition of the cosmic radiation in terms of $\langle \ln(A) \rangle$. The $\langle \ln(A) \rangle$ at energy E is the weighted average of the logarithmic atomic masses of the cosmic rays:

$$\langle \ln(A) \rangle = \sum f_A \ln(A)$$

where A is the atomic mass of the nucleus and f_A its fraction in the cosmic-ray flux.

In figure 10 are shown 3 profiles of $\langle \ln(A) \rangle$ re-

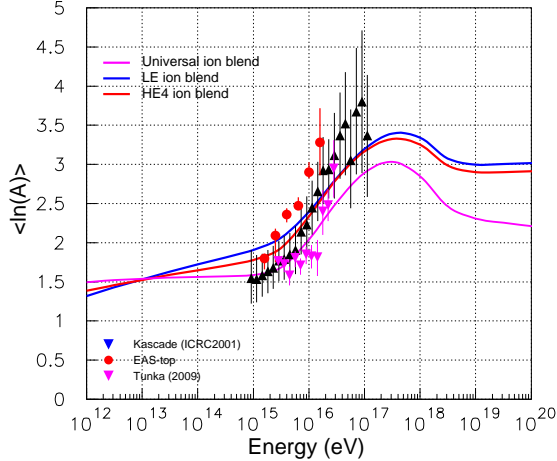


Figure 11. Comparison of the theoretical $\langle \ln(A) \rangle$ for the *LE* and *HE4* blends with that measured by Cascade (black triangles) [28] using the deconvolution method and that measured by Eas-top (red dots) [29].

sulting from 3 different ion blends: *LE*, *HE4* and the universal blend. The differences in the *LE* and *HE4* blends are quite negligible in the entire interval 10^{12} - 5×10^{19} . There are significant similarities but also some differences. The 3 profiles are similar in the band 2×10^{15} - 2×10^{17} eV, they all increase by about 2 units of $\langle \ln(A) \rangle$ and, in the range 5×10^{17} - 5×10^{18} , they all descend by about one unit. Differently, the $\langle \ln(A) \rangle$ profile of the universal blend is flat from the initial energy at 10^{12} up to 2×10^{15} eV, then it increases reaching a maximum of 3.05 at 2.97×10^{17} eV, and a more pronounced descent at high energy, and then, above 5×10^{18} eV, a modest decreasing trend dominates. The form of the $\langle \ln(A) \rangle$ profile of the *HE4* blend increases up to a maximum value of 3.33 at 3.94×10^{17} eV, then it decreases rapidly up to $(4-5) \times 10^{18}$ eV leveling off at higher energies around 2.8. As explained elsewhere (see fig. 4 of ref. [1]) the spectra of heavy ions (Ca and Fe) attain the low asymptotic plateaux (see fig. 7 and 8) at higher energies than the light ions. Low asymptotic plateaux reflect also the quasi rectilinear propagation in the Milky Way.

Figures 11 and 3 show data on $\langle \ln(A) \rangle$ of the Cascade experiment which separates all nuclei in

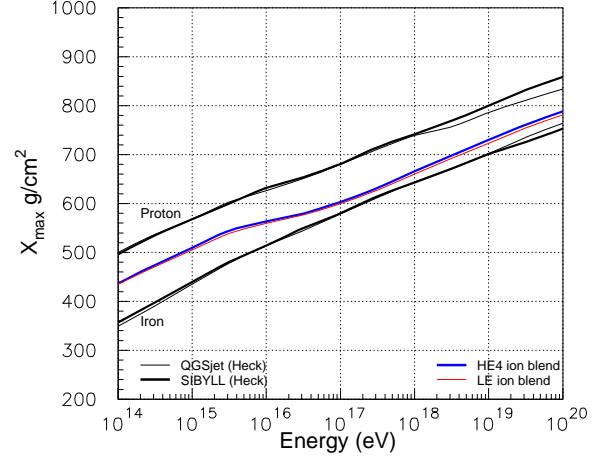


Figure 12. Atmospheric depths of shower maxima of protons and Fe nuclei versus energy computed by QGSjet and Sibyll hadronic codes as evaluated by Heck [30].

5 groups along with the corresponding theoretical curves (*LE* and *HE4*). The Eas-top data on $\langle \ln(A) \rangle$ are also shown in figure 11. Though there are discrepancies in the ion spectra in figure 3 obtained by QGSjet and Sibyll algorithms of the Cascade experiment [11], the resulting $\langle \ln(A) \rangle$ profiles show the correct general trends also observed by other experiments. By correct trend is meant an average increase of 1.5 units of $\langle \ln(A) \rangle$ in the interval 10^{15} - 10^{17} eV from an initial value of 1.8 at 10^{15} eV dictated by the extrapolation of balloon and satellite data at lower energies. The forms of the $\langle \ln(A) \rangle$ profiles in figure 11 obtained by the method of deconvolution [?] do not disagree with those of QGSjet and Sibyll algorithms shown in figure 3, though the $\langle \ln(A) \rangle$ in some energy bands have notable differences for the 3 methods. The agreement of the theoretical $\langle \ln(A) \rangle$ profiles for the *LE* and *HE4* blends with the Cascade data has been described in detail elsewhere [6].

At energies larger than 10^{17} eV the determination of chemical composition of the cosmic radiation becomes more involved because ions are not resolved individually nor in restricted groups. In order to determine the $\langle \ln(A) \rangle$ from the observables of the atmospheric showers recorded by

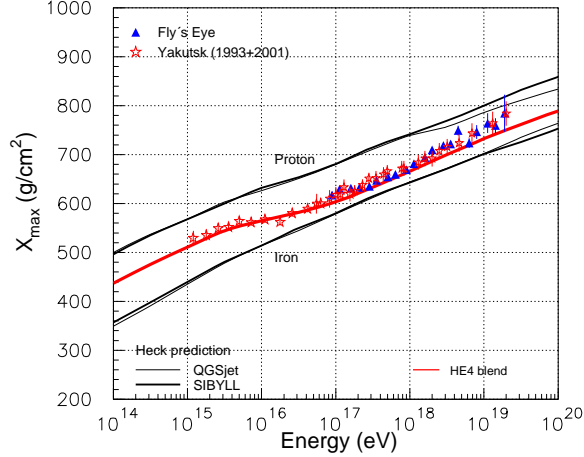


Figure 13. Atmospheric depths of shower maxima X_{max} versus energy measured by Fly's Eye (blue triangles) [31] and Yakutsk (red stars) [32] experiments compared with the corresponding theoretical profile (red line).

detectors, accurate and detailed models of the nucleus-air interactions are required. Traditionally, the depth in g/cm^2 of the maximum of the atmospheric showers (i.e. number of particles versus cascade axis) is denoted X_{max} or equivalently *elongation*.

A number of methods have been devised to measure X_{max} : (1) muon number and muon density detected at ground; (2) the mean width of the X_{max} distribution denoted in short $\sigma(X_{max})$; (3) Cherenkov light generated in the cascades; (4) fluorescence light generated in the cascades; (5) curvature of the cascade front measured by time-of-flight techniques. Apparata exploiting Cherenkov and fluorescence light can be equipped with additional detectors.

Figure 12 gives the X_{max} versus energy evaluated by Heck [30] for two models of nuclear interactions denoted in short QGSjet and Sibyll. It results that the depth of the maximum of the atmospheric showers induced by primary cosmic proton goes from $500 g/cm^2$ at 10^{14} eV to $850 g/cm^2$ at 10^{18} eV. In the same energy interval the Fe elongation goes from $350 g/cm^2$ at 10^{14} eV to $750 g/cm^2$ being the total thickness of the

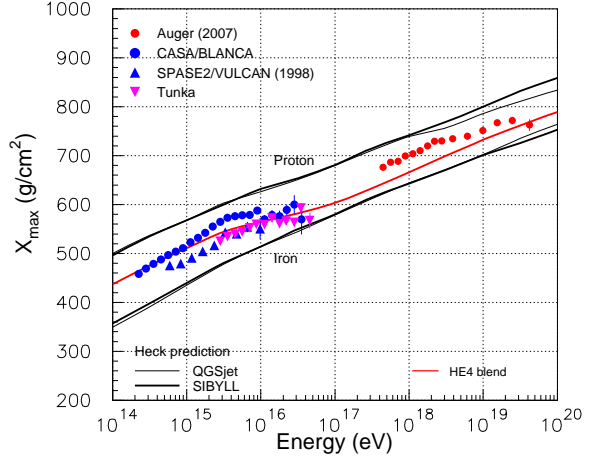


Figure 14. Atmospheric depths of shower maxima of protons and Fe nuclei versus energy measured by Auger, Space2/Vulcan [33] and Casa-Blanca [34] experiments compared with the $\langle \ln(A) \rangle$ profile derived from the theory.

air about $1000 g/cm^2$.

Above 10^{14} eV the gap between the proton X_{max} profiles of Sibyll and QGSjet regularly enlarges reaching $40 g/cm^2$ at 10^{20} eV (see fig. 12).

According to some simplifications the elongation is given by:

$$X_{max} = D((\ln E/E_0) - \ln(A)) + C$$

where X_{max} is the atmospheric depth in g/cm^2 , for primary particles of energy E , E_0 is a reference energy, $\langle \ln(A) \rangle$ the chemical composition and C and D two appropriate functions. Let us note that in the present calculation, unlike others, C and D vary with energy. In the following, in the comparison with the experimental data, both X_{max} and $\langle \ln(A) \rangle$ are maintained since the two variables are affected by small differences. The function $X_{max}^A(E, E_0)$ is the elongation for the nucleus A with the energy E normalized at the energy E_0 .

The function $X_{max}^A(E, E_0)$ obtained by cascade simulations depends on the hadronic models used

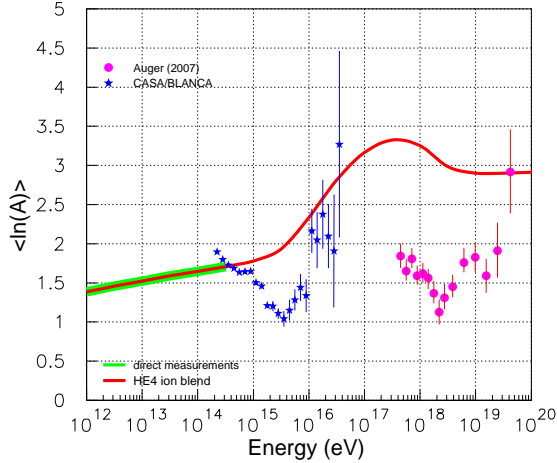


Figure 15. Chemical composition in terms of $\langle \ln(A) \rangle$ extracted by the X_{max} measured by Casa-Blanca [34] and Auger experiments. The $\langle \ln(A) \rangle$ profiles of each experiment curiously exhibit prominent depressions at 4×10^{15} eV and $(2 - 3) \times 10^{18}$ eV. The Casa-Blanca depression is probably due to an instrumental effect as argued in the text.

to describe the interactions of cosmic nuclei with the air. Once the experimental value of the elongation X_{max}^{exp} has been determined, the value of $\langle \ln(A) \rangle$ is obtained in the superposition model by the equation:

$$\langle \ln(A) \rangle = \ln(56) \times (X_{max}^H - X_{max}^{exp}) / (X_{max}^H - X_{max}^{Fe})$$

being X_{max}^H and X_{max}^{Fe} the elongations simulated by Monte Carlo for protons and Fe nuclei, respectively. Using the above equation, the $\langle \ln(A) \rangle$ derived from the theory can be converted into X_{max} . The result is shown in figure 12 with the blue and red curves which are the average value of X_{max}^H and X_{max}^{Fe} profiles obtained by QGSjet and Sibyll codes.

The Yakutsk [32] and Fly's Eye [31] data on $\langle \ln(A) \rangle$ are shown in figure 13 and they rep-

resent an example of accord between theory and data. Note that at energies above 10^{18} eV the theoretical X_{max} profile has a substantial gap with the data. The accord below 10^{18} eV and the discrepancy at high energy have been discussed in the companion paper [6].

Figure 14 reports examples of disagreement. The X_{max} measured by Auger [15] above 10^{17} eV exhibits a large discrepancy between data and theory in the huge interval $4 \times 10^{17} - 10^{19}$ eV. Subsequent elaborations of the Auger data samples [?] mark the stability of the X_{max} except for the last data point which decreases by about 5 g/cm^2 . The Casa-blanca and Space2/Vulcan data points in figure 14 have opposite deviations with respect to the theory, in different energy intervals.

The measurements of the atmospheric depths of the cosmic radiation made by Auger has been converted into $\langle \ln(A) \rangle$ and shown in figure 15. According to these measurements cosmic rays around 4×10^{18} eV mainly consist of 37 per cent of heavy ions. This figure comes from the partition of the cosmic nuclei in two groups, light and heavy (see subsequent Section 8).

Besides the Auger experiment, a notable structure in the $\langle \ln(A) \rangle$ profile, shown in figure 15, has been also observed by the Casa-Blanca experiment in the interval $10^{14} - 4 \times 10^{16}$ eV. The depression of $\langle \ln(A) \rangle$ measured by Casa-Blanca in the energy band $(3 - 9) \times 10^{15}$ eV would imply the disappearance of heavy elements. This depression corresponds to the decreasing difference between the measured X_{max} profile and the theoretical X_{max}^H in the interval $2 \times 10^{14} - 3 \times 10^{15}$ eV as shown in figure 14. As a consequence, the depression of the Casa-Blanca experiment shown in figure 15 is not a spurious effect in the conversion of X_{max} into $\langle \ln(A) \rangle$. This circumstance favours an instrumental effect and not a physical cause for the origin of the depression. The conclusion is corroborated by the measured by the Cascade Collaboration with 3 methods (fig. 3 and 11) and others experiments which, contrary

to Casa-Blanca data, register the disappearance of light elements.

6. Ion abundances outside the disc volume

In order to determine the ion abundances in the space outside the disc volume it is necessary to calculate the probability of escaping from the disc, P_E , for any individual ions at all energies. At very high energy, as ions propagate almost rectilinearly, this calculation is extremely simple.

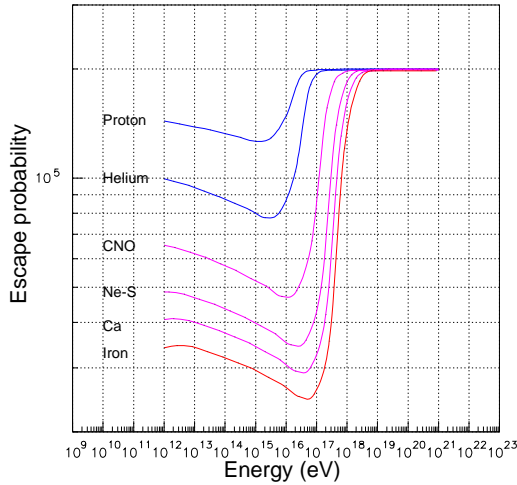


Figure 16. Probability of escaping from the disc P_E as a function of the energy for particles having cosmic-ray sources distributed uniformly in the disc volume [12]. The probability P_E is normalized to 2×10^5 particles.

Let E_A^d be the energy above which ions of mass A propagate almost rectilinearly in the disc. In the rectilinear propagation regime ions encounter a minimum amount of matter as evaluated elsewhere [3].

The amount of matter experienced by ions while propagating in the disc is referred to as

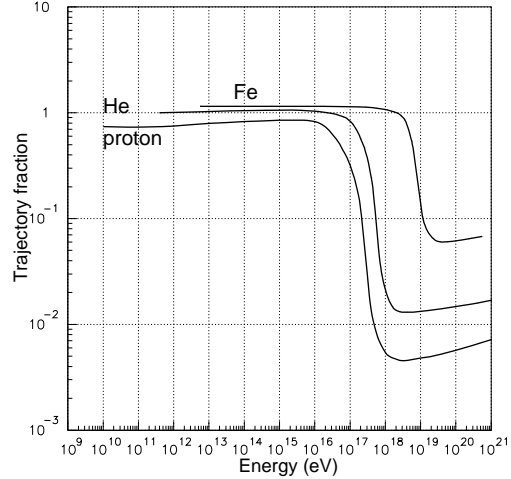


Figure 17. Number of nuclear collisions versus energy occurring in the disc volume for nuclei (H, He and Fe) having all the initial points of the trajectories placed in the solar cavity.

grammage, g . It is given by: $g=mnL$, where m is the mean atomic mass in the disc, n is the average number of atoms per cm^3 in the interstellar space and L the trajectory length. The grammage depends on nuclear cross sections via trajectory length, L . Since for $E > E_A^d$ the grammage is only $0.006 g/cm^2$, the number of nuclear collisions taking place in the disc is negligible, and consequently, ion abundances released by the cosmic-ray sources are almost unmodified when they are observed in the solar cavity.

Unlike the rectilinear propagation regime in the energy interval where $E < E_A^d$, between the knee and the ankle energy region, e. g. 3×10^{15} - 5×10^{18} eV, the galactic magnetic field affects ion motion, bending and inverting efficiently ion directions. This effect of the magnetic field for each ion makes the average grammage encountered by cosmic rays dependent on particle momentum. For $E < E_A^d$, the calculation of P_E and the probability for cosmic ions of entering (or re-entering) from the disc boundary to the solar cavity, P_R , is more involved and difficult. In the following the

functions P_R are determined.

The number of particles escaping from the disc N_F versus energy for 6 ions or group of ions is given in figure 16. The quantity N_F is normalized at the same number (2×10^5) of emitted particles (becoming the probability P_E). All curves in figure 16 have a minimum at a particular energy E_e^{min} (e is for escape). The characteristic energies where the minima of the 6 ions H, He, N, Si, Ca and Fe occur are, respectively : 1.1×10^{15} eV, 2.6×10^{15} eV, 1.2×10^{16} eV, 2.4×10^{16} eV, 3.9×10^{16} eV, and 4.5×10^{16} eV. The decreasing segment of N_F from 10^{12} eV up to E_e^{min} is due to the increasing nuclear cross sections with energy while the rising segment above E_e^{min} is predominantly caused by the vanishing efficiency of the galactic magnetic field with rising energy to retain particles for long times.

Escaped particles populating the extradisc space may re-enter the disc in the scheme delineated in Section 2, in a variety of circumstances. Let be P_R the mean probability for ions of energy E of reaching the Earth from the disc boundary. A cosmic-ray trajectory consists of an initial point (the source) and a termination point, which is the location where the nuclear collision occurs within the disc volume. The calculation of P_R exploits the approximate symmetry of the cosmic-ray trajectories contained in the disc volume between the initial point X_I and the final point X_F of the trajectory. Samples of 2×10^5 particle are injected from the solar system position and the trajectories reconstructed in the disc volume. Let N_I be the number of ions stopping in the disc volume by nuclear collisions and N_T the total number of trajectories (or injected particles). The function N_I is of fundamental importance in the present calculation since it incorporates the effect of the magnetic field, the dimension of the disc, the variation of the nuclear cross sections with the energy and the position of the solar system in the Galaxy. The calculation is finally accomplished by taking advantage of the inversion of the particle trajectories, the interchange of X_F with X_I , as explained in detail elsewhere [35]

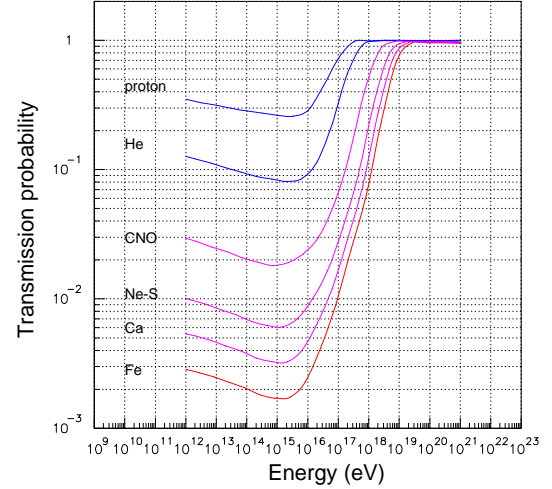


Figure 18. Probability of reaching the solar system for cosmic nuclei having all the initial points of the trajectories placed at the disc boundary.

Figure 17 reports the functions N_I for 3 representative ions H, He and Fe taken as reference examples. The N_I profile of any ion has a high plateau, a quite small rise controlled by nuclear cross sections, a rapid and high descend, a minimum, and finally, a modest increase up to the highest energies. For example, the number of He interactions in the disc, in the interval 5×10^{11} - 10^{15} eV, increases by 3.5 per cent. At 10^{12} eV the number of He particles interacting in the disc volume is 173000 out of 200000 injected from the Earth (hence, $N_T=2 \times 10^5$ and $N_I=1.73 \times 10^5$). At 5×10^{18} eV where the minimum of N_I for He nuclei occurs, the number of He interactions reduces to 2000 (hence $N_I=2000$). Therefore, the probability for He particles of reaching the solar cavity, having the initial points of the trajectories at the disc boundary, is : $P_R = 1 - (N_I/N_T)$. With the figures given above, the probability P_R is 0.11 at 10^{12} eV and 0.99 at 10^{18} eV. By this procedure the 6 probability functions versus energy P_R are obtained and shown in figure 18. The number of nuclear collisions taking place in the disc volume shown in figure 17 (see figure 6 of ref. [1]) is converted in terms of probability P_R in figure 18. The normalization of the functions

in figure 17 is explained in detail on the investigation on the origin of the knee (Section 4 of ref. [3]). Thus, the functions in figure 17 are closer to the simulation of the cosmic-ray trajectories and they facilitate the comprehension of the processes causing the ion knees [3], while those in figure 18 more specifically relate to the present study.

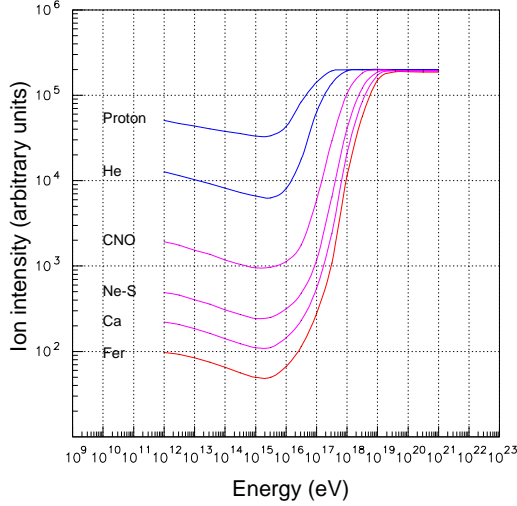


Figure 19. Particle fraction, f , versus energy of the extradisc component reaching the solar cavity from the disc boundaries (Halo of the Milky Way). The quantity f is defined as $f=N_e T$ where N_e is the number of particles escaped from the disc and T the transmission probability (see fig. 18) from the disc boundaries to the solar cavity at a specified energy.

Figure 20 is an illustration of how ion abundances of the extradisc component are affected by small variations of the spectral indices at the sources for cosmic ions migrating from the disc into the extradisc space. The abundances of H, He and Fe ions in the extradisc volume at 10^{19} eV are taken with the arbitrary ratios of 1.5, 1 and 0.33 (see fig. 20). Note that the three black curves (H, He and Fe) in fig. 20 are the same reported in figure 16 except for a different normalization. The Helium index γ_{He} is taken as a reference value (any value, including $\gamma_{He}=0$)

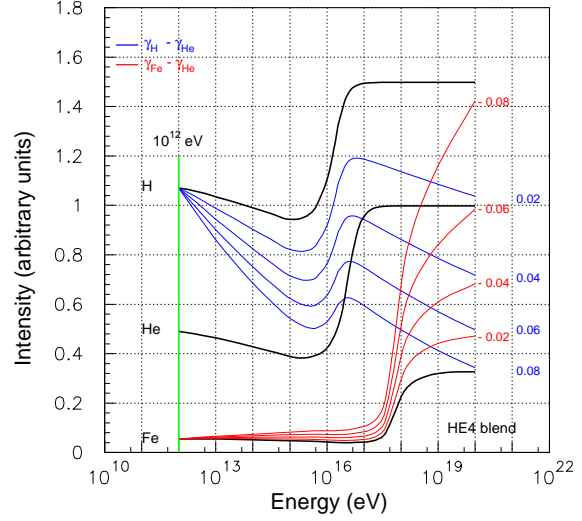


Figure 20. Small differences of $\pm 0.1\%$ in the spectral indices at 10^{12} eV will reverberate large alterations of the ion abundances around the ankle energy region. The grid of red and blue curves, specifying H and Fe ion abundances versus energy, result from the change, by arbitrary steps of 0.02 of the H and Fe indices, with respect to the He index taken as reference value (see text for details).

while the Fe and H indices are varied by small amounts of 0.02, 0.04, etc. with respect to γ_{He} , in order to map how ion abundances vary with energy. The result is displayed in figure 20 by the grid of red and blue curves in the interval $10^{12}-5 \times 10^{19}$ eV. For example, with a change of 0.08 in the index, the H/Fe abundance ratio of 19.9 (arbitrary value) at 10^{12} eV becomes 0.23 at 10^{19} eV, a factor 86.5 minor. Such a figure represents a large variation of the chemical composition. Note that at very high energy, above 10^{19} eV, the abundance ratios outside the disc volume are the same existing at the cosmic-ion sources in the disc, since particle displacement is unaffected by nuclear collisions, due to the small grammage traversed.

Measurements of the spectral indices in the energy region $10^{11}-10^{15}$ eV acquire a fundamental

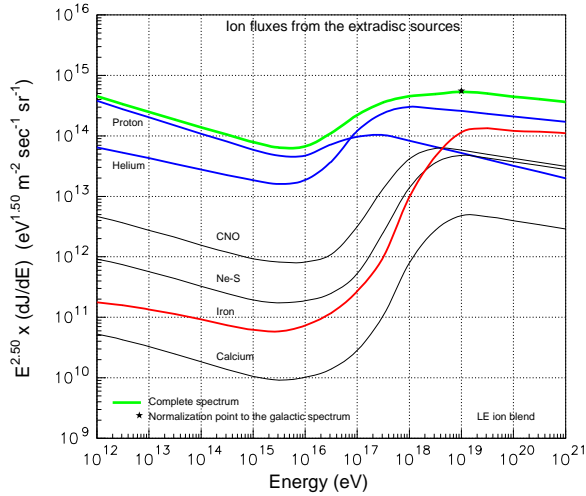


Figure 21. Energy spectra of the extradisc ions reaching the solar cavity emitted by sources characterized by the *LE* blend. The black star defines the flux normalization.

importance because their values determine the chemical composition at very high energy. The postulate of *Constant Spectral Indices*, incorporating the balloon and satellite data below 10^{15} eV, relates the chemical composition at low energy to that at very high energy by logical necessity avoiding any *ad hoc* mechanisms, at small, arbitrary energy bands, to explain the chemical composition of the cosmic radiation.

7. The Chemical composition of the extradisc component

The chemical composition of the extradisc component is radically different from that of the disc component. Heavy ions, escaping from the disc volume and penetrating through the disc of the Milky Way from its exterior, pay twice a tribute to larger nuclear interaction cross sections with respect to light ions. Therefore, the heavy-to-light ion flux ratio inevitably augments above 10^{15} eV up to the ankle energy region.

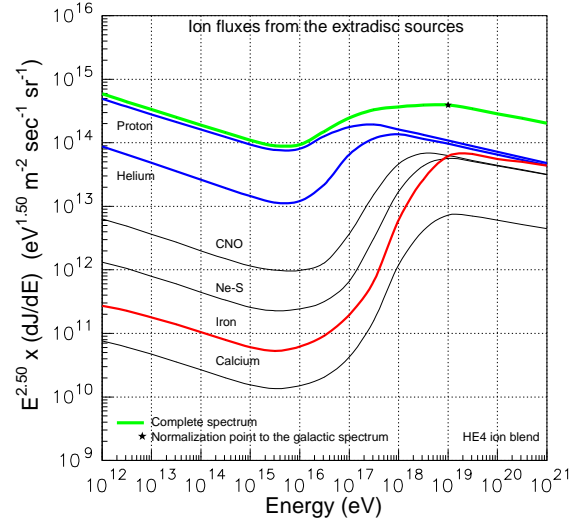


Figure 22. Energy spectra of the extradisc ions reaching the solar cavity emitted by sources characterized by the *HE4* ion blend. The black star signals the flux normalization.

Figures 21 and 22 report the energy spectra of the extradisc ions reaching the solar cavity for the two *LE* and *HE4* blends. Firstly, note that a simplified situation takes place above the maximum of the Fe energy spectrum located at 2×10^{19} eV. The ion abundances above this energy coincide with those at 10^{12} eV reported in Table 1. Above 2×10^{19} eV the grammage is so small that nuclear interactions in the interstellar medium do not alter the chemical composition of the extradisc component existing at the outskirts of the disc volume. The complete spectrum in figure 21 and that in figure 22 are normalized at the arbitrary energy of 10^{19} eV to the galactic flux of 5.35×10^{14} (*LE*) and 3.91×10^{14} (*HE4*) particles/ m^2 sr s $eV^{1.5}$.

Figure 23 shows ion fractions versus energy of the extradisc component for 3 groups of ions: light, intermediate and heavy being, respectively, (H+He), (CNO + Ne-S) and (Ca + Fe). This ion partition is adopted in some experiments. Let us now analyze the ion fraction profiles starting from the extreme high energy where the situation

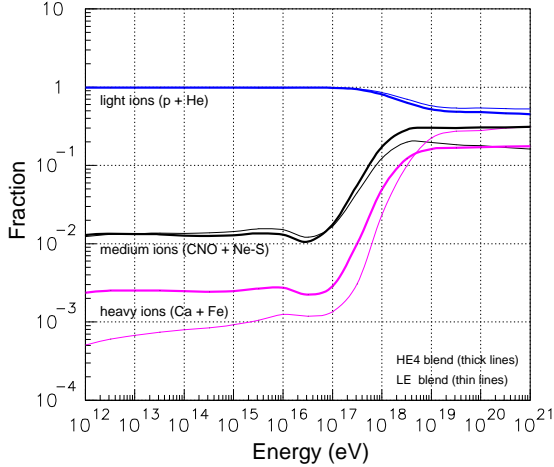


Figure 23. Relative amounts of light, intermediate and heavy ions versus energy for the *LE* (thin curves) and *HE4* (thick curves) ion blends generated by the extradisc component.

is simpler.

Just above 2×10^{19} eV ion abundances of the extradisc component reaching the solar system are equal to those of the cosmic-ray component present in the parent galaxy, because particle displacement through the disc (escaping and entering) do not alter ion abundances. Around 2×10^{19} eV terminates the increase of 2 orders of magnitude of the (Ca+Fe) ion fraction. The (Ca+Fe) fraction above 5×10^{18} eV does not surpass 17 per cent, even with an increase of a factor 66 from the low level flat fraction, below 5×10^{16} eV. The intermediate ions, i.e. the sum of CNO and (Ne-S) group of nuclei, has a similar pattern with a step, between the low and high level, of a factor 25, which constitutes 31 per cent of the extradisc component above 5×10^{18} eV.

From the profiles of the ion fractions shown in figure 23 or from the more detailed ion spectra shown in figures 21 and 22, the $\langle \ln(A) \rangle$ of the extradisc component is directly calculated; it is shown in figure 24 (pink curve, *HE4* blend). The

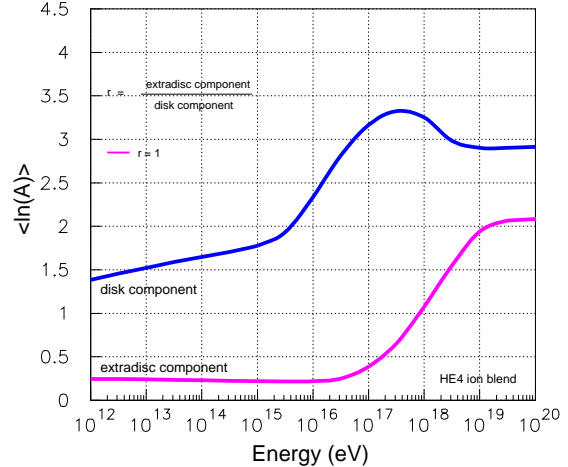


Figure 24. Chemical composition in terms of $\langle \ln(A) \rangle$ versus energy of the disc (blue curve) and extradisc component (pink curve) for the *HE4* ion blend derived from the *Theory of Constant Spectral Indices*.

same figure 24 shows, for visual comparison, the corresponding $\langle \ln(A) \rangle$ resulting from the disk component (blue curve, blend *HE4*), which has a quite different pattern. The $\langle \ln(A) \rangle$ for the *LE* blend of I_{ed} has a quite similar pattern (fig. 10). The two $\langle \ln(A) \rangle$ profiles of the disc and the extradisc components in figure 24 are normalized at the same cosmic-ray intensity at Earth.

The $\langle \ln(A) \rangle$ of the extradisc component exhibits a constant value below 5×10^{16} eV, followed by a rising trend in the interval 5×10^{16} - 2×10^{19} eV with an approximate constant slope. Above 2×10^{19} eV the $\langle \ln(A) \rangle$ stabilizes to the constant value of 2.1. The physical phenomena shaping this silhouette have already been discussed. A simplified, instant, qualitative comprehension might be depicted in terms of grammage encountered by the cosmic rays during the displacement in the Galaxy. When the grammage is large (see figure 16 ref. [3]) heavy nuclei are destroyed, when the grammage is minimum (0.006 g/cm^2) heavy nuclei travel undisturbed like light

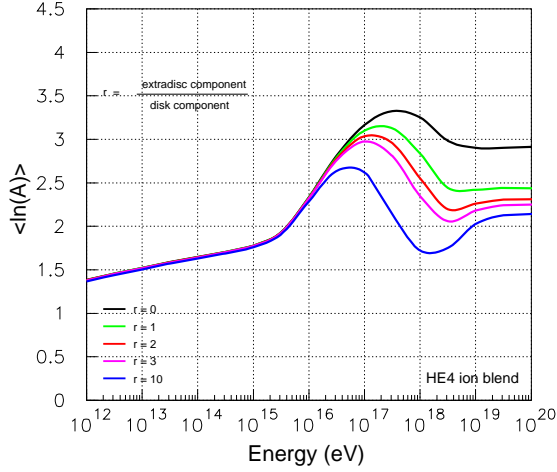


Figure 25. Chemical composition in terms of $\langle \ln(A) \rangle$ versus energy for various values of the extradisc-to-disc flux ratios, r , for the *HE4* ion blend.

nuclei and the persists unchanged regardless of the energy. In the intermediate region 5×10^{16} - 2×10^{19} nuclear cross sections and geometrical factors compete and interplay, forging the chemical composition with the stable, rising trend shown in figure 24.

When the disc and extradisc components are combined together for different values of $r = I_{ed}/I_d$, it results the surprising $\langle \ln(A) \rangle$ profiles shown in figure 25. For $r=1$ the flux in the solar cavity is 1.8×10^{14} particles/(m^2 sr s $eV^{1.5}$) at 10^{19} eV for both disc and extradisc components. The surprising aspect of the $\langle \ln(A) \rangle$ profiles in figure 25 resides in the fact that they thoroughly resemble to the profile of the experimental data on $\langle \ln(A) \rangle$ extracted from the measurements of X_{max} of the Auger experiment.

Flux measurements of the cosmic radiation at Earth imperatively constraint r , the maximum value of the extradisc component, as evident in figure 26. The sum of the fluxes of the disc and extradisc components is shown in figure 26 along

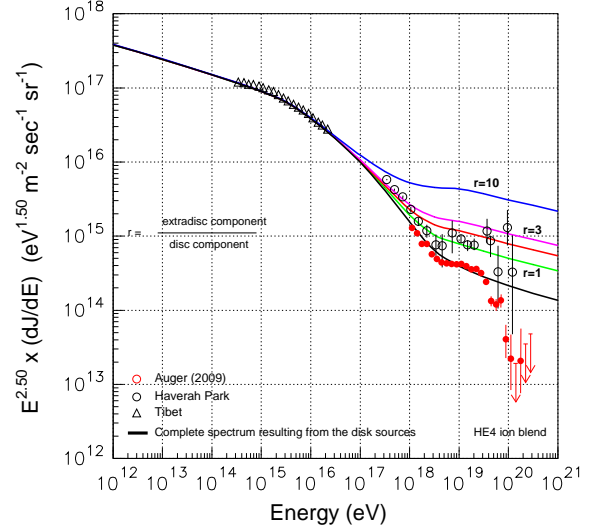


Figure 26. Energy spectra of the cosmic radiation with different values of the extradisc-to-disc flux ratio, r , derived from the *Theory of Constant Indices* framed between the Haverah Park and Auger flux measurements.

with flux data of two experiments, taken as an example. Magnifying the extradisc component to match the Auger data on $\langle \ln(A) \rangle$ would entail a conflict with the observed fluxes.

Notice that the theoretical spectra in figure 26 intrinsically exhibit the adequate change in the slope around 4×10^{18} eV, from 3.2 to 2.7, which constitutes the ankle. Similarly, around 10^{15} eV, the slope of the complete spectrum changes from 2.7 to about 3.0 which is a characteristic features of the knee.

With the assumptions adopted in this paper any types of extradisc component generate a rather light chemical composition below 10^{17} eV due to the dominant role of nuclear cross sections suffered by heavy ions while propagating from periphery to disc core.

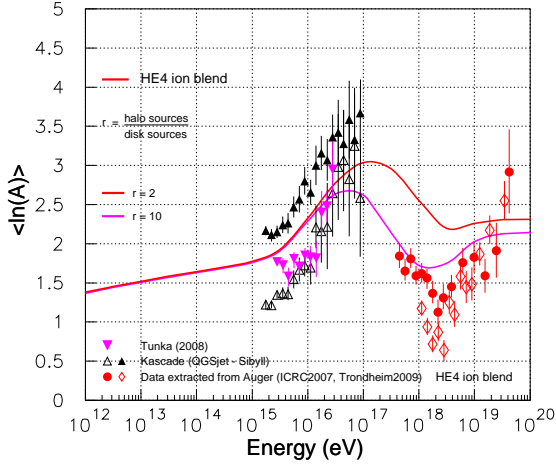


Figure 27. Comparison of the theoretical profiles of $\langle \ln(A) \rangle$ (red and pink curves) with the empirical one extracted from the X_{max} measured by the Auger experiment (red diamonds and dots). The extradisc-to-disc flux ratio at 10^{19} is 2 (blue line) and 10 (pink line).

8. Comparison between theoretical and measured $\langle \ln(A) \rangle$ with the disc and extradisc components

In the following the experimental data on $\langle \ln(A) \rangle$ are compared with the profile derived from the theory in the condition $r=2$. Note that the $\langle \ln(A) \rangle$ in the the condition $r=1$ or $r=3$ would describe the experimental data as well, due to the large systematic uncertainties inherent to the hadronic models describing atmospheric showers. The value $r=2$ is regarded here as a adequate compromise between cosmic-ray intensity (see fig. 26) and the depth of the minimum of the $\langle \ln(A) \rangle$ profile (see fig. 25).

In all the subsequent figures 27, 28, 29, 30, 31, 32, and 33, where high energy data on $\langle \ln(A) \rangle$ above 10^{17} eV are examined and compared with the theory, the $\langle \ln(A) \rangle$ determined by the Cascade experiment in the range 10^{15} - 10^{17} eV is dis-

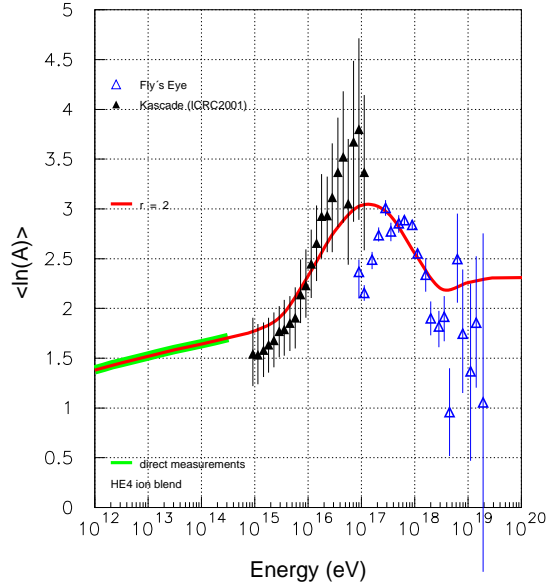


Figure 28. Comparison of the theoretical profile of $\langle \ln(A) \rangle$ (red curve) with the empirical one extracted from the data of Fly's Eye experiment (blue triangles).

played as adequate, reference measurement.

From the Cascade Collaboration three different procedures to determine $\langle \ln(A) \rangle$ are available called here Sybill algorithm, QGSjet algorithm and deconvolution method. Data of the first two methods are in figure 3 and 27 while those of the deconvolution method, which covers the largest range, i.e. 9×10^{14} - 1.4×10^{17} eV, are in figure 28. The resulting $\langle \ln(A) \rangle$ profiles from the three methods of measurement by Cascade are simultaneously shown elsewhere (see figure 24 of ref. [11]) exhibiting a coherent silhouette in the entire interval 10^{15} - 10^{17} eV.

Recent measurements of X_{max} of the Auger Collaboration converted into $\langle \ln(A) \rangle$ by the reference profiles for H and Fe shown in figure 14 are given in figure 27. Two predicted $\langle \ln(A) \rangle$ profiles according to the *Theory of Constant Indices* with $r=2$ and $r=10$ are shown in fig. 27. In the condition $r=2$ the Auger data in the interval 4×10^{17} - 10^{19} eV are still below the theoretical

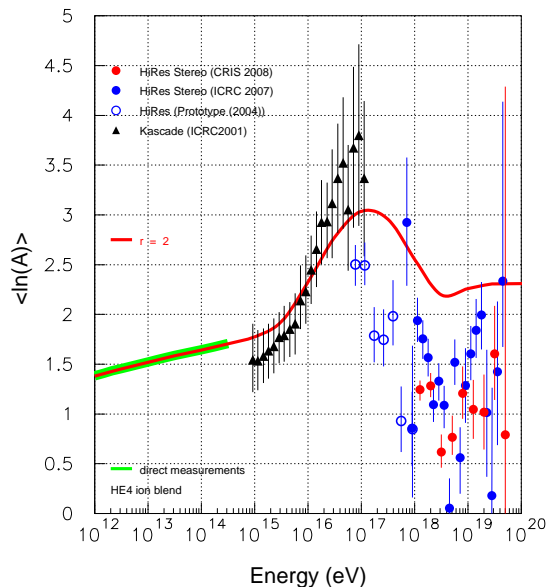


Figure 29. Comparison of the theoretical profile of $\langle \ln(A) \rangle$ (red curve) with the empirical one extracted from the data of HiRes experiment before (blue data points) and after (red data points) acceptance corrections.

profile.

The $\langle \ln(A) \rangle$ extracted from the X_{max} measured by the Fly's Eye experiment [31] is shown in figure 28. The increasing trend of $\langle \ln(A) \rangle$ in the interval 10^{17} - 6×10^{17} eV contrasts with the opposite trend of HiRes and Agasa-Akeno experiments (see figs. 29 and 32); it also disagrees with a flat silhouette observed by Yakutsk in the same energy interval, and with a value of 3.5 measured by Cascade. The behavior of $\langle \ln(A) \rangle$ in figure 28 is reminiscent of that observed by the Haverah Park experiment (see fig. 31) in the same energy interval, where a lack of uniformity in the detector acceptance is suspected.

The profile of $\langle \ln(A) \rangle$ extracted from the X_{max} measured by the HiRes experiment is shown in figure 29. The HiRes data in figure 29 include HiRes Prototype [36], HiRes Stereo [37] and a data revision which takes into account acceptance correction and detector performance

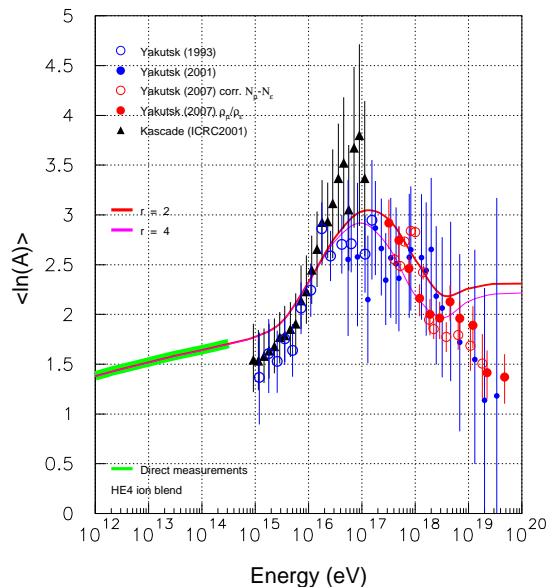


Figure 30. Comparison of the theoretical profile of $\langle \ln(A) \rangle$ (red curve) with the empirical one extracted from the data of the Yakutsk experiment (blue small circles).

[38]. Around 4×10^{18} eV data reported in figure 29 have a mean value of $\langle \ln(A) \rangle$ of about 1. This tiny value would correspond to the minimum observed by Auger at $(2 - 4) \times 10^{18}$ eV as far as a vague increase of $\langle \ln(A) \rangle$ would delineate in the band 5×10^{18} - 4×10^{19} eV. The chemical composition extracted from the X_{max} measured by HiRes is lighter than that resulting from the highest permissible values of the parameter r (dominance of extradisc component) in the interval 10^{17} - 10^{19} eV. It is also lighter, by about one unit of $\langle \ln(A) \rangle$, than that of Auger, Fly's Eye, Haverah Park and Agasa experiments (see figure 4 of ref. [39].)

The profile of $\langle \ln(A) \rangle$ extracted from the X_{max} measured by the Yakutsk Collaboration [32] is shown in figure 30. There is a global, remarkable agreement with the theory in the huge interval 10^{15} - 10^{19} eV characterized by a bell-shaped profile with a maximum of $\langle \ln(A) \rangle$ of 3 around the energy of 2×10^{17} eV. Above 5×10^{18} eV data would suggest the lightning of the chem-

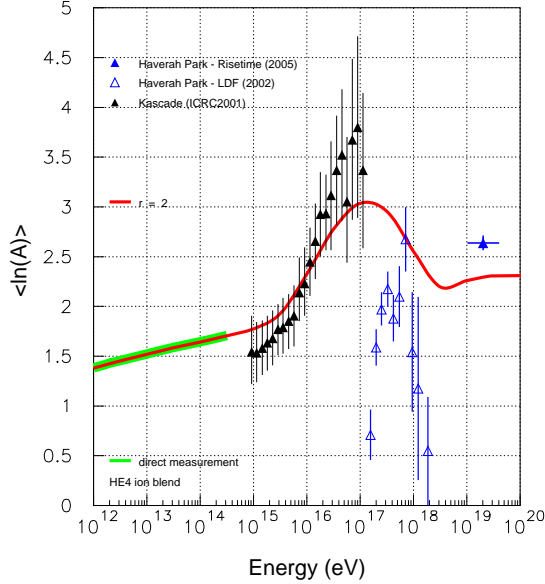


Figure 31. Comparison of the theoretical profile of $\langle \ln(A) \rangle$ (red curve) with the empirical one extracted from the data of the Haverah Park experiment (blue triangles).

ical composition. Notice, by contrast, that the chemical composition of measured by Auger in the interval $5 \times 10^{18} - 4 \times 10^{19}$ eV would indicate the opposite trend: the $\langle \ln(A) \rangle$ becomes heavier according to the data shown in figure 27.

9. Comparison between theoretical and measured $\langle \ln(A) \rangle$ in Haverah Park, Agasa and Volcano Ranch

The partition of the cosmic nuclei in two groups, light and heavy, with fractions F_p and F_{Fe} respectively, characterizes the chemical composition extracted from Haverah Park, Agasa and Volcano Ranch data samples. This bi-modal data analysis, though appropriate for some detectors, has a clear bias since it gives intrinsically higher $\langle \ln(A) \rangle$ than realistic ion groupings as demonstrated below.

The chemical composition measured by the

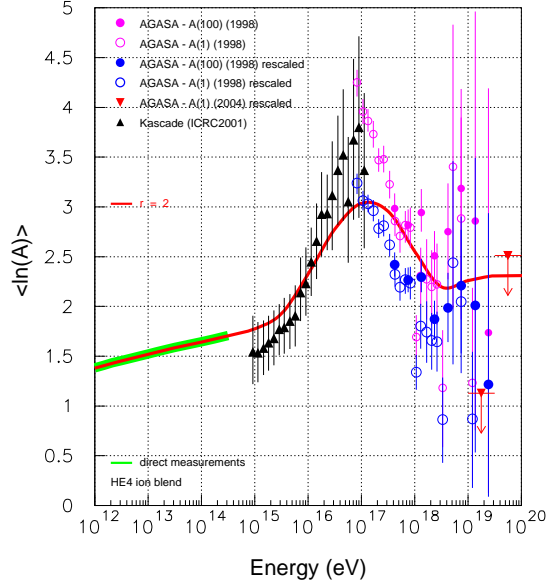


Figure 32. Comparison of the theoretical profile of $\langle \ln(A) \rangle$ (red curve) with the empirical one extracted from the data of Agasa experiment (blue and pink data points).

Haverah Park experiment is reported in figure 31. Ruling out the data points at the extreme energies, below 2×10^{17} eV and above 10^{18} eV, where detector acceptance for atmospheric showers might have been deteriorated (See Section 3 ref. [40]), the agreement with the theoretical $\langle \ln(A) \rangle$ profile in the condition $r=2$ is excellent. For protons and Fe nuclei the differences in the theoretical X_{max} profiles shown in figure 12 for Sibyll and QGSjet codes are small in the interval $10^{17} - 10^{18}$ eV, and so the agreement between theory and Haverah Park data is quite stable. It has been remarked [41] the critical role of hadronic models in the partition of all cosmic-ray nuclei in two classes, light (F_p) and heavy (F_{Fe}). Adopting the code *QGSjet98* it results a proton fraction F_p of .34 while the code *QGSjet01* gives $F_{Fe} = 0.48$ [41].

Data samples collected by the Agasa Collaboration have been revisited in 2003 [42] in order to determine the X_{max} of the cosmic radiation in the range $10^{17} - 10^{20}$ eV. The chemical composition re-

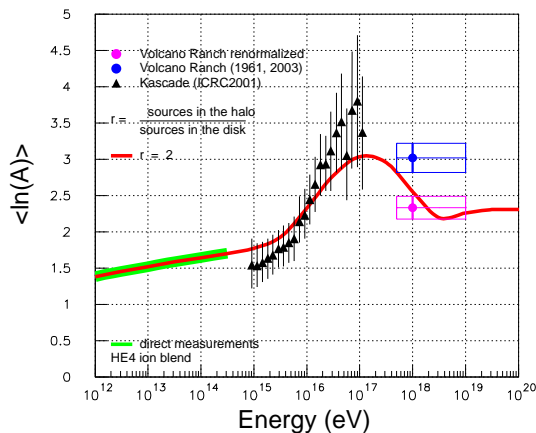


Figure 33. Comparison of the theoretical profile of $\langle \ln(A) \rangle$ (red curve) with the empirical one extracted from the data of Volcano Ranch experiment (blue cross in the rectangle). The data point corrected according to the *Theory of Constant Spectral Indices* is represented by a pink cross in the rectangle.

sulting from this data re-elaboration [42] is shown in figure 32 by blue squares. The global profile of the empirical $\langle \ln(A) \rangle$ in figure 32 would resemble to that measured by Auger in a significant aspect: $\langle \ln(A) \rangle$ decreases above the energy of 10^{17} eV up to $(2 - 3) \times 10^{18}$ eV, where a minimum is attained. In the interval $2 \times 10^{18} - 2 \times 10^{19}$ eV, with some imagination, an increasing trend would faintly delineate, being in accord with the $\langle \ln(A) \rangle$ profile of the Auger experiment above 3×10^{18} eV (see fig. 27).

The partition of atmospheric showers in two groups according to the quoted re-analysis of the Agasa data [42] has been here refined with 6 particles (or 6 ion groups) giving the outcome shown in figure 32 by pink square data points. In this refinement the *Theory of Constant Spectral Indices* with the HE4 blend has been used. The resulting $\langle \ln(A) \rangle$ profile (pink squares in fig. 32) is systematically shifted downward by about one unit

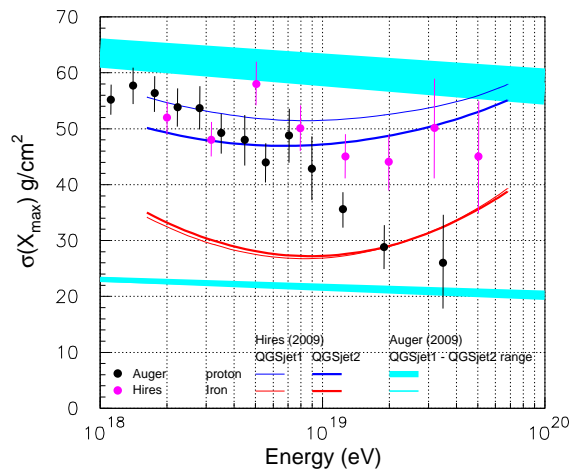


Figure 34. Measurements of the chemical composition of the cosmic radiation by HiRes (pink dots) and Auger (black dots) experiments using the mean width of the longitudinal profile of the fluorescence light generated in atmospheric showers. The theoretical mean width in g/cm^2 versus energy evaluated by Heck [30] for protons and Fe nuclei with QGSjet and Sibyll algorithms is also shown as turquoise bands.

of $\langle \ln(A) \rangle$. To appreciate numerically such a shift, just caused by the refinement with 6 ion groups instead of 2, consider that a Fe fraction of 0.60 implies a $\langle \ln(A) \rangle$ of 2.41 ($A = 56$). The HE4 blend at the energy of 10^{19} eV for the 6 ions H, He, CNO, Ne-S, Ca and Fe with fractions, respectively, of .22, .21, .16, .16, 0.02 and 0.23 gives a $\langle \ln(A) \rangle$ of 2.26. The LE blend at 10^{19} eV with the ion fractions of .08, .41, .10, .09, 0.01 and 0.31 gives a $\langle \ln(A) \rangle$ of 2.43.³

³Unfortunately, an heavy ion fraction F_{Fe} higher than 1 results in figure 4 of ref. [42], which signals a logical incoherence whatsoever in the data elaboration materializing an unphysical situation. The incoherence is not easy to be eliminated since reverberates elsewhere [46]. Probably, an additional correction of a few g/cm^2 in the X_{\max}^{cal} derived from the Mocca-Sibyll code would eliminate the Fe fractions higher than 1 in fig. 4 of the quoted reference [42] or in fig. 4 of ref. [44]. Note that this additional correction probably is unnecessary since the oversimplified data elaboration with only two ion groups (instead of 6 or more) entails a bias in $\langle \ln(A) \rangle$ which is clearly demonstrated

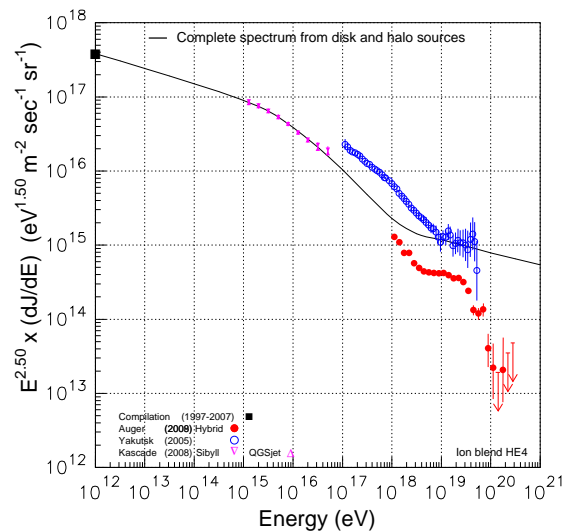


Figure 35. Evidence for the present uncertainties in cosmic-ray flux measurements in different experiments using giant terrestrial cascades in air above 10^{17} eV. The spectrum (black curve) resulting from the *Theory of Constant Spectral Indices* is normalized at 10^{12} eV (black square) with a flux of 3.79×10^{17} particles/(m^2 sr s $eV^{1.5}$) and it joins the KASCADE data in an excellent accord.

A consistency verification of the chemical compositions derived from the Agasa-Akeno data [43] and that extracted by X_{max} measured by Fly's Eye has been performed in 1998 [44]. Both the radial muon density from the cascade core ρ_μ and the X_{max}^{cal} have been simulated with the same hadronic code, Mocca-Sibyll. Calculations have been adapted to Akeno (A1), Agasa (A100) and Fly's Eye detectors including muon thresholds, trigger efficiencies and other instrumental constraints, which are significant. Grouping all nuclei in two fractions, light and heavy, so that $F_p + F_{Fe} = 1$, it results a fraction F_{Fe} greater than 1 for the Fly's Eye data around 10^{17} eV. In order to remove this incoherence a shift of -30 g/cm^2 in the X_{max}^{cal} is required. The interesting aspect of this correction is that the theoretical profile X_{max}^{cal} resulting from Mocca-Sibyll code differs from that used in this paper (see figure 12) by about 25

in figure 32 or in figure 33 with the Volcano Ranch data.

g/cm^2 at 10^{17} eV, and similarly at higher energies. Such a difference would alleviate, as a gratuity, the gap between the $\langle \ln(A) \rangle$ predicted by the *Theory of Constant Spectral Indices* with $r=2$ and the Auger data (see fig. 27).

An elaboration and revision of atmospheric shower data of Volcano Ranch experiment operated in the period 1959-1964 has been performed in 1975 using a bi-modal analysis [45]. Figure 33 shows the theoretical profile (red curve) along with the data point of Volcano Ranch (blue rectangle) spanning the interval 5×10^{17} - 10^{19} eV. The resulting $\langle \ln(A) \rangle$ has a mean value of 3, which indicates that the cosmic radiation at 10^{18} eV is still dominated by intermediate and heavy nuclei. If the same procedure of ion ponderation applied to the Agasa data is also applied to Volcano Ranch data with the HE4 ion blend, the mean value of $\langle \ln(A) \rangle$ decreases from 3 to 2.4 (pink cross in the rectangle) approaching the theoretical value of 2.5 as displayed in figure 33.

10. Reported measurements of the mean atmospheric depth of the cosmic radiation by fluorescence light in HiRes

Though the longitudinal profile of giant atmospheric showers reconstructed by the fluorescence light is rather insensitive to the hadronic models employed in the data analysis, it would seem that some instrumental unknowns or uncontrolled measurement procedures still plagues the determination of X_{max} by fluorescence light.

Preliminarily, notice that experiments taking advantage of the fluorescence light in the measurements of X_{max} like HiRes do not agree one another. The X_{max} observed by the HiRes experiment [38] is larger than that measured by Auger [15] which uses the fluorescence light as well. As an example, the Fly's Eye data on $\langle \ln(A) \rangle$ [31] in the energy decade 3×10^{17} - 3×10^{18} eV shown in figure 28 differ from those of HiRes Prototype

(figure 29) by one unit of $\langle \ln(A) \rangle$ which is quite large by any standard, theoretical, empirical or instrumental.

The measurements of X_{max} by fluorescence light demands the interpolation of the longitudinal profile by an appropriate function f_{LP} which has a characteristic width denoted here $\sigma(X_{max})$. The average value of the distribution of $\sigma(X_{max})$ at a given energy is a measurement of the chemical composition. The observed $\sigma(X_{max})$ may be cross-check method in the measurements of the chemical composition with the same data samples.

Presently (2009), the available measurements of $\sigma(X_{max})$ of the HiRes Collaboration [47] disagree with the analogous data of the Auger experiment [48] as shown in figure 34. Note that the theoretical $\sigma(X_{max})$ profiles shown in figure 34 derive from the same sample of the simulated cascades used to calculate the X_{max} profiles of figure 12. The $\sigma(X_{max})$ profile measured by HiRes is rather flat around the value of 50 g/cm^2 in the interval 10^{18} - 5×10^{19} eV while Auger data (full black dots) exhibit a clear decreasing profile from a maximum of 58 g/cm^2 down to a minimum of 22 g/cm^2 . Imagine a linear scale of energy between 10^{18} - 5×10^{19} eV in figure 34 and the disagreement between the two experiments dilates, since the initial agreement below 4×10^{18} eV is confined in less than 5 per cent of the explored energy band.

At the energy of 10^{17} eV the profile of $\langle \ln(A) \rangle$ measured by Cascade joins that of the HiRes experiment [36] (fig. 29). The average value of the $\langle \ln(A) \rangle$ of the Cascade experiment is about 3.1 (average value of 3 methods of measurements) while that of HiRes is close to 2.5. It is important to emphasize the disagreement, or the potential disagreement, between these two experiments on $\langle \ln(A) \rangle$ around 10^{17} eV. The knees of the light ions have been observed by a number of experiments above 10^{15} eV [49,50]. This fact necessarily implies an increase of $\langle \ln(A) \rangle$ above 10^{15}

eV, since the disappearance of light ions automatically enhances the heavy ion fraction. Knowing that at 10^{15} eV the value of $\langle \ln(A) \rangle$ is certainly comprised between 1.74 and 1.78 as inferred by extrapolating balloon and satellite data [52], any estimate of $\langle \ln(A) \rangle$ at 10^{17} eV leads to the value of 3.1 and not a lower value as HiRes Prototype data (2004) [36] around 10^{17} eV in figure 29 would suggest.

As apparent in figure 29 the mean values of $\langle \ln(A) \rangle$ of the HiRes experiment after the acceptance correction [38] are globally displaced downward by some 0.5 units. The shift is surprisingly large compared to the reported error bars before and after acceptance corrections [38]. The large excursions in $\langle \ln(A) \rangle$ (blue dots) also signal that the global detector performance suffered from residual uncontrolled unknowns.

The correction of the detector acceptance [38], a routine effect applied after 3 years from the original measurement [37] does not preclude future data re-analysis.

In synthesis, the HiRes data pertaining the chemical composition of the cosmic radiation disagree ⁴: (1) with the Auger data on X_{max} ; (2) with the Auger data on $\sigma(X_{max})$ (see figure 34 and the related text); (3) with those of all other experiments on $\langle \ln(A) \rangle$ above 10^{17} eV (Volcano Ranch, Haverah Park, Akeno, Agasa, Fly' s Eye and Yakutsk); (4) with the Cascade data at 10^{17} eV. Theoretically, a bias exists in the conversion of X_{max} into $\langle \ln(A) \rangle$ made by the HiRes Collaboration because, out of all current versions of

⁴ The resonance of this conclusion tunes up with the criticism expressed by A. A. Watson [51] on Fly's Eye and HiRes experiments: «... By contrast, with fluorescence detectors the aperture continues to grow with energy and remains considerable uncertainty about the HiRes aperture. Extensive Monte Carlo calculations must be made to establish it and these make assumptions about the slope of the spectrum and about the primary mass, with protons being assumed on the basis of the claims from the Fly' Eye and HiRes experiments ignoring often contradictory evidence from other experiments without discussion ».

hadronic codes adopted to simulate nuclear interactions in air (e.g. QGSjet, Sibyll, etc.), those adopted by HiRes tend to generate protons and depress heavy ions (see fig. 8 of ref. 10 and fig. 4 ref. [39]).

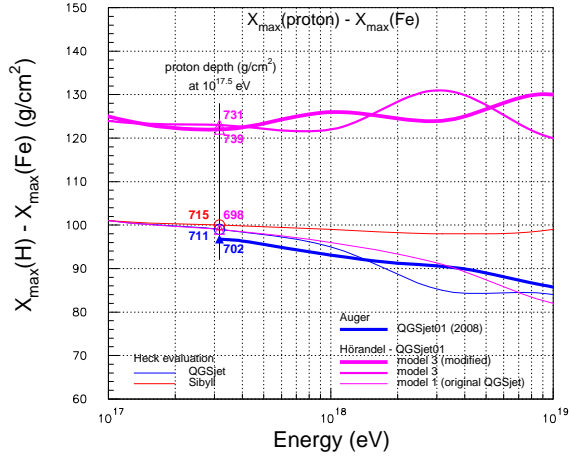


Figure 36. Theoretical difference of the atmospheric depth for protons and Fe nuclei according to a number of evaluations. The model QGSjet-03 (thick pink curve) [52] would reduce the discrepancy between Auger data on $\langle \ln(A) \rangle$ and the corresponding profile derived from the *Theory of Constant Indices*.

11. Conclusions.

The comparison of the chemical composition of the cosmic radiation expressed by $\langle \ln(A) \rangle$ derived from the *Theory of Constant Indices* with the observed $\langle \ln(A) \rangle$ extracted from the Auger data on X_{max} dictates the necessity of introducing an extradisc component of the cosmic radiation above 10^{17} eV. In Sections 1 and 2 it is explained why this component is better termed *extradisc component*, I_{ed} . The variable r is a free parameter of the theory defined as the extradisc-to-disc flux ratio in the solar cavity at 10^{19} eV,

e.g. $r = I_{ed}/I_d$.

From the ensemble of the profiles of $\langle \ln(A) \rangle$ extracted from the measurements of X_{max} of the Auger, Yakutsk, Fly' s Eye, Agasa, Akeno, Haverah Park and Volcano Range experiments it emerges a global accord with the theory.

In the energy interval 10^{15} - 10^{17} eV there is an excellent agreement with the observations of Eastop, Cascade, Tunka (see fig. 3) and other experiments. Below 10^{17} eV the extradisc component is a negligible fraction of the disc component I_d , and as a consequence, the theoretical and empirical analysis reported in the companion paper [8] remains valid.

Because of the unknowns entailed in the conversion of X_{max} into $\langle \ln(A) \rangle$ above 10^{17} eV, the accord between the theoretical profile and data in figures 27, 28, 30, 31, 32 and 33 is more than satisfactory. Values of $r = I_{ed}/I_d$ higher than 2 would alleviate the gap between the empirical profile of $\langle \ln(A) \rangle$ and the theory, as shown in figure 27. Presently, values of r higher than 2 are neither convincing nor necessary, due to large systematic errors in the experimental data. The last two figures 35 and 36 intend to illustrate this position.

Figure 35 depicts in a flash the present experimental uncertainties in flux measurements quoting arbitrarily data from Cascade, Yakutsk and Auger experiments. Fluxes from other experiments do not agree as well. Such uncertainties impede to identify a more precise and reliable value of the ratio r in figure 26 on an empirical basis, being $r=2$ the present adequate global estimate.

Let be $X_{max}^{cal}(\text{H})$ the theoretical atmospheric depth for protons, $X_{max}^{cal}(\text{Fe})$ that for Fe nuclei and D_{max} the difference between the two depths i.e. $D_{max} = X_{max}^{cal}(\text{H}) - X_{max}^{cal}(\text{Fe})$ at a given energy E . Error sources generating differences in $\langle \ln(A) \rangle$ in theories and in experiments might

arise both from X_{max}^{cal} (H) and D_{max} as well. Ideally, different hadronic models may result in a combination of X_{max}^{cal} (H) and D_{max} having the same $\langle \ln(A) \rangle$. Figure 36 reports the D_{max} versus energy in some current hadronic models and, at the arbitrary energy of $10^{17.5}$ eV, the X_{max}^{cal} (H). Figures 36 and 12 show that the X_{max}^{cal} (H) and D_{max} profiles used in this paper for the conversion of X_{max} into $\langle \ln(A) \rangle$ are quite similar to those adopted by others (for example, Auger).

Notice that the hadronic code called QGSjet model-03 [52], having a larger D_{max} of 120-130 g/cm^2 in the relevant range 10^{17} - 5×10^{19} eV and a deeper X_{max}^{cal} (H) of 739 g/cm^2 at $10^{17.5}$ eV (see figure 36), it would shift upward the simulated X_{max} profiles in figure 12 by 9 g/cm^2 at $10^{17.5}$ eV. The same correction applied to the Auger data in figure 3 (or figure 14) would shift upward by 0.57 units of $\langle \ln(A) \rangle$ (9 g/cm^2 for $r=0$ or 11 g/cm^2 for $r=2$) at 4.12×10^{17} eV alleviating the gap between Auger data and theory. As far as uncertainties in hadronic models above 10^{17} eV used in the analysis of giant atmospheric cascades remain large, the determination of a value of r higher than 2 based on the $\langle \ln(A) \rangle$ data would appear premature. This same conclusion is suggested by the flux measurements in figure 35.

Let us finally mention the systematic disagreement between the $\langle \ln(A) \rangle$ extracted from the X_{max} measured by the HiRes experiment and theory, amounting to about one unit in the entire interval 10^{17} - 5×10^{19} eV (see fig. 29). The examination of the HiRes data on $\langle \ln(A) \rangle$ made in Section 9 suggests a number of inconsistencies with the data of numerous experiments and with different versions of the HiRes experiment itself (HiRes Prototype, HiRes Stereo, data revision [38]).

REFERENCES

1. A. Codino and F. Plouin, CRIS 2006, Nucl. Phys. B (Proc. Sup.) **165** (2007) 307-316.
2. A. Codino and F. Plouin, Proc. Vulcano Conf. (2006), 403 and astro-ph/0701521.
3. A. Codino and F. Plouin, INFN Report/TC-06/05 (2006), 4th February 2006, Lab. Naz. di Frascati, Frascati, Italy; astro-ph/0701498 (2007).
4. A. Codino and F. Plouin, Proc. 30th ICRC, Merida, Mexico, **576** (2007).
5. A. Codino, *The Naked Iron Knee, its Necessity and Empirical Evidence*, INFN Report/TC-09/05, 31st July 2009, Lab. Naz. di Frascati, Frascati, Italy.
6. A. Codino and F. Plouin, CRIS 2008, Nucl. Phys. B (Proc. Sup.) **190** (2009) pages 228-239, Salina Island, Italy.
7. W. D. Apel et al., (Kascade Coll.) astro-ph/0804.4274v.1, 27th April 2008.
8. M. A. Lawrence et al. (Haverah Park Coll.), Proc. 21th ICRC, Adelaide, Australia, **3** (1990) 159; M. Ave et al., astro-ph/0112253 (2002, data revision).
9. M. Aglietta (EAS-top Coll.), Astropart. Phys. **20** (2004) 641.
10. R. Engel, (Kascade Coll.) astro-ph/0504358, 15 april 2005.
11. A. Codino, *Proton and Helium fluxes and the Origin of the Knee in the Spectrum of the Cosmic Radiation*, INFN Report/TC-09/06, 15th October 2009, Lab. Naz. di Frascati, Frascati, Italy.
12. M. T. Brunetti and A. Codino, The Astrophys. Jour., **528** (2000) 789.
13. V. V. Prosin et al., (Tunka Collab.) 18 ECRS Conf. session EP 1a 4; CRIS2008 Salina Island, Italy (2008).
14. J. R. Hörandel (Kascade Coll.), Aspen, Colorado, USA (2005), J. of Phys., Conf. Series **47** (2006) 41 and astro-ph/0508014.
15. M. Unger et al., (Auger Coll.) Proc. 30th ICRC Merida Mexico 594 and astro-ph/0706.1495 (2007).
16. A. Codino and F. Plouin, Proc. 30th ICRC, Merida, Mexico (2007), **703**.

17. B. Wiebel-Sooth, astro-ph/9709253 (1997).
18. A. D. Panov et al., (Atic Coll.) Astro-ph/0612377, January 2006.
19. Eo Yun Suk Seo (Cream Coll.), Proc. 30th ICRC Merida (2007), **677**.
20. P. Boyle, (Tracer Coll.), Proc. 30th ICRC, Merida Mexico (2007) **1192**.
21. R. Bellotti et al., (MASS Coll.), Phys. Rev. D, **60**, 052002 (1999).
22. Y. S. Yoon et al., (Cream Coll.) Proc. 31th ICRC Lodz, Poland (2009) **00668**.
23. N. L. Grigorov et al., Proc. 12th ICRC, vol. 5, Hobart, 1971, page 1746.
24. A. Haungs, (Kascade Coll.), Astro-Alice Workshop, CERN, 15th june 2003.
25. M. Roth et al., (Kascade Coll.), Proc. 28th ICRC, Tsukuba, Japan (2003).
26. Guido Pizzella, Nature **226** (1969) 434.
27. K. Asakimori et al., (Jacee Coll.) The Astrophys. Journ. **502** (1998), 278.
28. K. H. Kampert et al., (Kascade Coll.), astro-ph/0204205v1, 12th April 2002.
29. M. Aglietta et al., (Macro and Eas-top Coll.), Astropar. Phys., **21** (2004) 583-596.
30. D. Heck quoted in S. P. Swordy et. al., Workshop held at Adler Planetarium, Chicago (2000); (a) astro-ph/0103073 (QGSjet). (b) Proc. 29th ICRC, Pune, India (2005) 135 (QGSjet-01c, QGSjet-II). (c) T. Pierog et al., Proc. 30th ICRC Merida, Mexico (2007) **899** (QGSjet-01, QGSjet-II03).
31. D. J. Bird et al. (Fly's Eye Coll.), The Astrophys. Jour., **424** (1994) 491.
32. S. Knurenko et al., (Yakutsk Coll.), Proc. 27th ICRC, Hamburg, Germany, **HE1.3** (2001) 145.
33. J. E. Dickinson et al. (Space2/Vulcan Coll.), Proc. 26th ICRC, Salt Lake City (USA), **3** (1999) 136.
34. J. W. Fowler et al., (Casa-Blanca Coll.) astro-ph/0003190v2 (2000) and Astropar. Phys. **15** (2001) 49.
35. A. Codino and F. Plouin, The Astrophys. Jour., **639** (2006) 173.
36. T. Abu-Zayyad et al. (HiRes Coll.), The Astrophys. Jour. , **557** (2001) 686.
37. R. U. Abbasi et al. (HiRes Coll.), The Astrophys. Jour., **622** (2005) 910.
38. Belz, (HiRes Coll.) Nuclear Physics B (Proc. Suppl.) **190** (2009) pages 5-11, Salina Island, Italy.
39. A. Codino, *Redundant Failures of the Dip Model of the Extragalactic Cosmic Radiation*, astro-ph/0911.4273v1, 22nd November 2009.
40. Ave et al., (Haverah Park Coll.) astro-ph/0203150 (2002).
41. M. Ave et al., (Haverah Park Coll.) Astropar. Phys. **61** (2003) 61.
42. M.T. Dova et al., Proc. 28th ICRC, Tsukuba, Japan (2003), page 377.
43. N. Hayashida et al., (Akeno Coll.) Journ. Phys. G, **61** (1995) 1101.
44. M. Dawson et al., (Akeno-Agasa Coll.), astro-ph/9801260.
45. M.T. Dova et al., Proc. 29th ICRC Pune, India (2005).
46. K. M. Simpson, *Studies of cosmic rays Composition Using a Hybrid Fluorescence Detector*, Thesis of University of Adelaide, Australia, May 2001.
47. P. Sokolsky, *Final HiRes Results and Telescope Array Experiment*, Conf. SOCoR 15-18 June 2009, Trondheim, Norway.
48. M. Unger et al., (Auger Coll.) *Study of the Cosmic Ray Composition with the Pierre Auger Observatory*, (Auger Coll.) Conf. SOCoR 15-18 June 2009, Trondheim, Norway.
49. M. Aglietta et al., (Macro and Eas-top Coll.), Astropar. Phys. **21** (2004) 583-596.
50. K. H. Kampert, CRIS2006, Catania, Nucl. Phys. B (Proc. Sup.) **165** (2007) 294-306.
51. A. A. Watson, Proc. CRIS2004, Catania, Italy.
52. J. R. Hörandel astro-ph/0309010, 1st September 2003.